NAA-SR-9720
COPY
87 PAGES

SNAP 10A PRESTARTUP AND STARTUP PERFORMANCE

(Title Unclassified)

AEC Research and Development Report

ATOMICS INTERNATIONAL
A DIVISION OF NORTH AMERICAN AVIATION, INC.

DISCLAIMER

LEGAL NOTICE

Printed in USA Price $1.85 Available from the

U. S. Atomic Energy Commission
Technical Information Extension,
P. O. Box 1001
Oak Ridge, Tennessee.

Please direct to the same address inquiries covering the procurement of other classified AEC reports.

NAA-SR-9720
SNAP REACTOR,
SNAP PROGRAM
M-3679 (34th Ed.)

SNAP 10A PRESTARTUP AND STARTUP PERFORMANCE

(Title Unclassified)

By

G.S. DRUCKER
T.J. BOYLE

ATOMICS INTERNATIONAL

A DIVISION OF NORTH AMERICAN AVIATION, INC.
P.O. BOX 309 CANOGA PARK, CALIFORNIA

CONTRACT: AT(11-1)-GEN-8
ISSUED: JUNE 30, 1964

DISTRIBUTION

SYSTEMS FOR NUCLEAR AUXILIARY POWER (SNAP)-REACTOR SNAP PROGRAM M-3679 (34th Ed.)

	No. of Copies
Aerojet-General Corporation (NASA)	1
Aerojet-General Nucleonics	1
Aeronautical Systems Division	2
Aerospace Corporation	1
Aerospace Test Wing (AFSC)	1
Air Force Weapons Laboratory	2
AiResearch Manufacturing Company, Phoenix	1
Army Ballistic Research Laboratories	1
Army Materials Research Agency	1
Army Missile Command	1
Army Nuclear Defense Laboratory	1
ARO, Inc	1
Air University Library	1
Argonne National Laboratory	1
Army Combat Developments Command	1
Astropower, Inc.	1
Avco Corporation	1
Battelle Memorial Institute	1
Bendix Corporation (AF)	1
Brookhaven National Laboratory	1
Bureau of Naval Weapons	2
Bureau of Ships	2
Bureau of Yards and Docks	1
California Patent Group	1
Central Intelligence Agency	1
Chicago Patent Group	1
Defense Atomic Support Agency, Sandia	1
Department of the Army	1
Director of Defense Research and Engineering (OAP)	1
Edgerton, Germeshausen and Grier, Inc., Goleta	1
Foreign Technology Division (AFSC)	1
General Atomic Division	1
General Dynamics/Astronautics (AF)	1
General Dynamics/Fort Worth	1
General Electric Company, Cincinnati	1
General Electric Company (FPD)	2
General Electric Company (MSVD)	1
General Electric Company, Richland	2
General Electric Company, San Jose	1
General Electric Company, San Jose (AF)	1
General Technologies Corporation	1
Institute for Defense Analysis	1
Ion Physics Corporation	1
Jet Propulsion Laboratory	2
Johns Hopkins University (APL)	1
Lockheed-Georgia Company	1
Lockheed Missiles and Space Company	1
Los Alamos Scientific Laboratory	1
Martin-Marietta Corporation, Denver	1
Monsanto Dayton Laboratory	1
NASA Ames Research Center	1
NASA Goddard Space Flight Center	2
NASA Langley Research Center	1
NASA Lewis Research Center	4
NASA Manned Spacecraft Center	1
NASA Marshall Space Flight Center	1
NASA Scientific and Technical Information Facility	3
National Aeronautics and Space Administration, Washington	1
NASA Western Operations Office	1
Naval Air Development Center	1
Naval Ordnance Laboratory	2
Naval Postgraduate School	1
Naval Radiological Defense Laboratory	1
Naval Research Laboratory	2
Naval Underwater Ordnance Station	1
Navy Marine Engineering Laboratory	1
New York Operations Office	1
New York Operations Office, Canel Project Office	1
North American Aviation, Inc , Downey	1
Nuclear Metals, Inc.	1
Office of Naval Research	2
Office of the Assistant General Counsel for Patents (AEC)	1
Office of the Chief of Engineers	1
Office of the Chief of Naval Operations	3
Office of the Chief of Naval Operations (OP-03EG)	2
Office of the Chief of Transportation	1
Phillips Petroleum Company (NRTS)	4
Pratt and Whitney Aircraft Division	1
Pratt and Whitney Aircraft Division (NASA)	1
Rand Corporation	1
Republic Aviation Corporation	1
Sandia Corporation	1
School of Aerospace Medicine	1
Union Carbide Corporation (ORNL)	8
USAF Headquarters	1
University of California, Livermore	1
Westinghouse Electric Corporation (NASA)	1
Division of Technical Information Extension	40
AI Library (Includes 2 copies to CPAO, 2 copies to AEC, Washington, 2 copies to COO)	69

CONTENTS

TABLES

FIGURES

FIGURES

BLANK

I. SUMMARY

One of the key features of the SNAP 10A design is the in-orbit startup capability of the system. This feature minimizes the problems of prelaunch handling and adds greatly to the nuclear safety of the system. The requirement for in-orbit startup introduces a number of design problems. These problems are discussed in this report and the results are presented to show that the present design will meet the requirement.

Prior to startup, it is necessary to ensure that a long-life orbit has been obtained. Therefore, the system must be capable of being started after 6 to 25 hr in a space environment. Since NaK, the heat transfer fluid, may freeze or plug during this period, the system is designed to limit the minimum NaK temperature to 50°F. An ejectable heat shield is used to ensure that the minimum temperature requirement is met. In addition, the maximum heat shield temperature is limited to 350°F, and the core outlet temperature of the NaK is limited to 225°F.

The heat shield operation is based on a low value of inside emissivity, which restricts the loss of heat from the radiator converter; and a high outside ratio of solar absorptivity to thermal emissivity, which causes the shield to take on a relatively high equilibrium temperature in the sun. The system temperature variations are kept to a minimum by circulating NaK at a rate of about 4% of the design value.

The space environment may be described in terms of two limiting cases; the sun-shade transient, and the constant sun-constant shade orbits. The environment description provides the heat inputs to the system thermal model which consists of a large number of heat balances on system heat transfer nodes. The system response is found by solving numerically the nonlinear equations of the model on a digital computer. The model was tested against ground test data obtained on the FSM-1 system. Good agreement was obtained between computed and measured values.

For the space environment, the results of the model predict a minimum NaK temperature of 61°F, a maximum core outlet temperature of 152°F, and a maximum heat shield temperature of 346°F. Thus, at nominal design conditions,

all system requirements are met. A parametric analysis was conducted to determine the effect of variations from nominal design conditions. Under "worst case" conditions, the only system requirement which is exceeded is the maximum heat-shield temperature. Tests are being conducted to determine if the shield will operate satisfactorily under the worst case conditions.

The function of the startup control system is to bring the SNAP 10A system from the subcritical low-temperature conditions of the prestartup period to rated power and temperature conditions. This must be done stably and without exposing the system to undue thermal stresses. The method used consists of the insertion of reactivity at a constant rate until the reactor outlet temperature attains a preset value. Thus, the principal controlled variable is the reactor outlet temperature, and the principal manipulated variable is control drum position.

The objective of the startup analysis is to determine the key startup parameters to ensure that a satisfactory startup can be made in orbit. Once startup with nominal parameters is demonstrated, the effects of variations of these values must be explored to ensure satisfactory operation over the expected range of variations. A detailed model of system behavior in the startup period has been used to meet these objectives. The model consists of the following:

a) Heat balances on system components

b) Nuclear and thermal equations of the reactor

c) Pump and NaK flow descriptions

d) Control system simulation

e) Environmental simulation

These equations were solved using a combination of digital and analog computation. The startup transients obtained may be divided into the following distinct regions:

a) A region during which neutron flux increases from the source strength level to a power level at which sensible heat effects are felt (about 100 watts)

b) An initial power transient during which the nuclear power and reactor temperature increase rapidly, then peak, as the reactivity feedback effects come into play

c) A longer term period during which the power and temperature slowly approach design conditions, then overshoot slightly when design conditions are reached.

The key factors in the transient response are the size of the initial power peak (and the corresponding peak temperature and rate of change of temperature); the size of the final power and temperature overshoot; and the stabilized power and temperature at the beginning of the 72-hr, active-control, full power period. The values predicted by the analysis for nominal design conditions are presented in Table 1. These results are completely consistent with the requirements on the startup control system. The parameter study did not reveal any problem areas because of variations from nominal conditions.

TABLE 1

RESULTS AT NOMINAL CONDITIONS

Initial power peak	56 kw
Peak temperature	420°F
Peak rate of change	9.5°F/sec
Final power overshoot	44 kw
Temperature peak	1030°F
Stabilized power	42.5 kw
Stabilized temperature	1017°F

To test the validity of the model used in the startup analysis, comparisons were made between model results and two ground tests. The nuclear reactor portion of the model was compared with results of tests on the SNAP 2 Developmental Reactor. The nonnuclear portions of the model were compared with the results of the FSM-1 system test. Good agreement was obtained in each case.

It has been concluded that the SNAP 10A system will satisfactorily meet all prestartup and startup system requirements.

BLANK

II. INTRODUCTION

A. SNAP 10A SYSTEM

A conceptual drawing of the SNAP 10A system is shown in Figure 1. The reactor is typical of the zirconium hydride-uranium fueled, SNAP type. The fuel chosen gives a high hydrogen density and, hence, small overall size and weight, and achieves the relative control simplicity typical of thermal neutron spectrum systems. The reactor core is reflected by beryllium and is controlled by four semicylindrical control drums operating in the reflector. These drums function by varying the neutron leakage flux. Sodium-potassium alloy (NaK-78) coolant circulates through the core, entering at 856°F and exiting at 986°F at nominal conditions. The overall reactor power required is 41 kw. This particular reactor type possesses a strong negative-temperature coefficient which is used for inherent control and stability over the operating lifetime, thus eliminating the need for continuous control-drum actuation. This static, or inherent, control system is possible because of

1) the rating of the reactor, which results in negligible reactivity shift due to fuel burnup, and

2) low reactor temperature, which minimizes the dissociation and subsequent loss of hydrogen from the fuel.

The heated NaK, upon leaving the core, is circulated at a rate of 4800 lb/hr by means of a liquid metal d-c conduction-type pump composed of a permanent magnet and an integral thermoelectric power supply. This power supply gives high current and low voltage, and consists of lead-tin-telluride (PbSnTe) thermoelectric materials which operate with a temperature difference established by the hot NaK temperature and a cold junction integral heat-rejection radiator. The hot NaK is then pumped to the thermoelectric power conversion system which converts, through the Seebeck effect, a portion of the thermal energy directly into electrical energy.

The power conversion system consists basically of N and P doped silicon-germanium (SiGe) thermoelectric materials thermally coupled but electrically isolated from the NaK heat-transfer medium. These SiGe pellets are bonded to 40 stainless-steel tubes arranged in a conical configuration about the structure. The NaK flow from the reactor is equally divided among the 40 tubes.

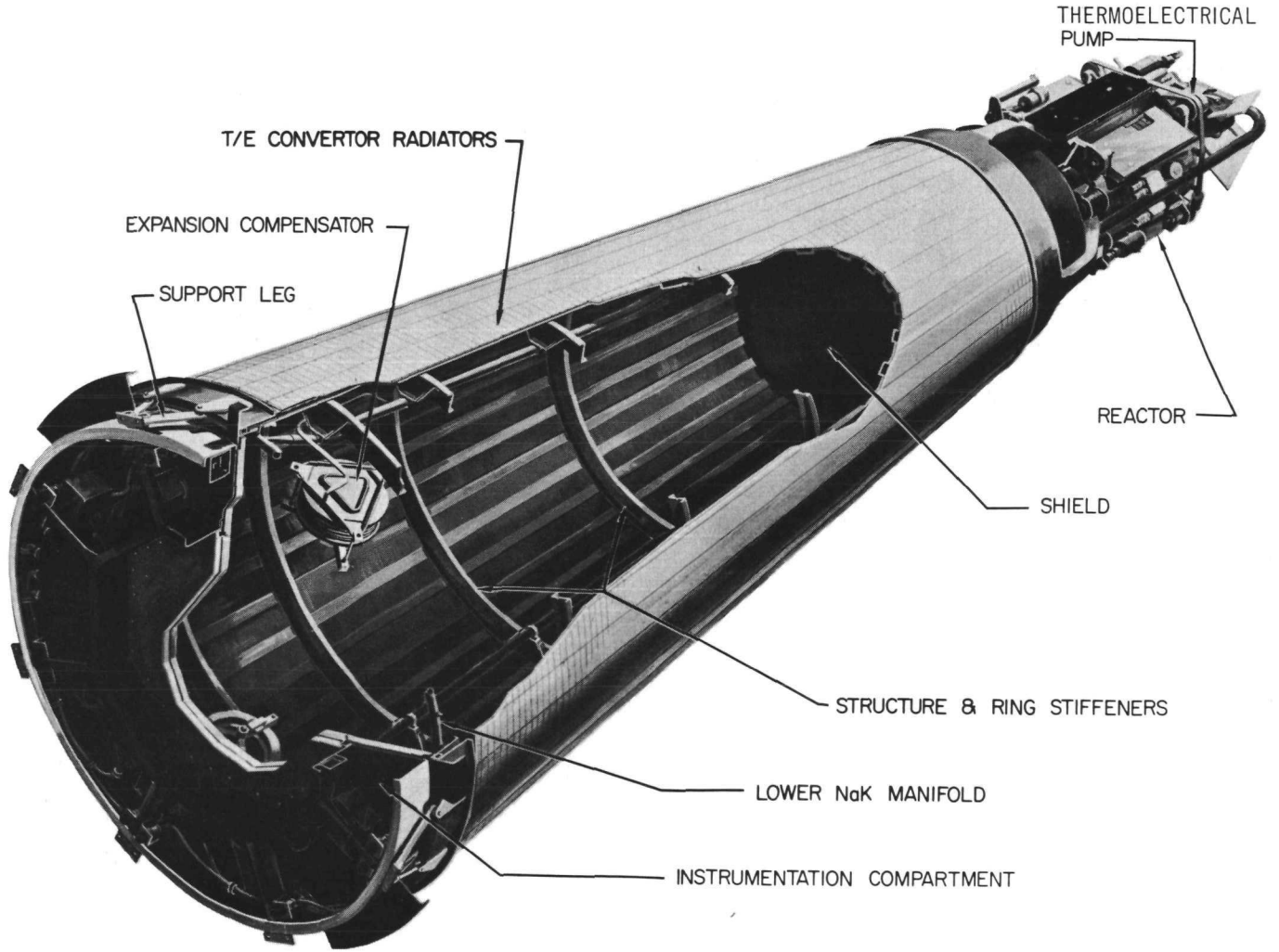

3-5-63

7561-0033D

Figure 1. SNAP 10A System

Along any one tube there are 72 SiGe pellets. These pellets are electrically isolated from the NaK tube by thin alumina discs. The heat transport path is from the NaK tube through the insulator, through the SiGe pellet, to an individual aluminum radiator. The total effective radiator area is 62.5 ft^2, and the radiator operates at a mean temperature of 600°F giving a power output of 510 watts. All materials which comprise the pellet subassemblies are brazed or otherwise metallurgically bonded to each other to ensure a sound structural and thermally conductive stack.

From the outlet of the power conversion system, the NaK coolant is collected and returned to the reactor core. Attached to the return legs are bellows-type expansion compensators which pressurize the system in orbit to 5 psi and maintain a void-free NaK volume.

The remaining components of the SNAP 10A serve to support, shield, start up, or diagnose the behavior of the basic system.

B. PRESTARTUP AND STARTUP SEQUENCE

The period of time covered by this report extends from the time of orbit injection until a satisfactory steady-state operating point is established. Initially, the system is at its prelaunch ambient temperature. At the end of the time period covered, the system will be at temperatures determined by its 990°F core outlet temperature. The reactor will go from a substantially subcritical condition to critical operation at a power level of 38 kw.

There are two distinct phases of this change in state. In the initial period, during which orbital parameters will be established, there will be no internal heat generation in the system. System temperatures will go from their initial ambient values to new temperatures of the order of 250°F under the influence of the thermal environment of space. In this mode, the response will be that of a semipassive system. The only active internal source will be a small amount of coolant flow induced by battery-supplied current flow to the NaK pump.

After it has been determined that the system is in a long-life orbit, the ground command will initiate a phase of active control. The system will be brought from the temperature distribution of the passive period and a subcritical state first to criticality and then, through continued control drum insertion, to a sensible heat condition in which the nuclear heat generation begins to raise

system temperatures. The system temperature will rise until the desired core outlet temperature is reached. The system then settles down to its design conditions. When a satisfactory equilibrium has been reached, the system reverts to a passive control mode at rated power conditions.

In the following sections, the two phases of operation described above are treated separately. The prestartup orbital period is studied with the aid of a digital computer program. The study of the startup period is accomplished with the aid of an analog computer program. It should be kept in mind that the analyses presented represent the final versions of a sequence of analyses which started with the preliminary design phase of the program.

III. PRESTARTUP ORBITAL ANALYSIS

A. DESIGN REQUIREMENTS AND HEAT SHIELD DESCRIPTION

The first stage in the operation of the SNAP 10A Nuclear Power Unit (NPU) is the verification of the orbital parameters to ensure that a long-life orbit has been attained. To achieve this verification, it is necessary that the NPU be capable of operating satisfactorily after a period of 6 to 25 hr in a space environment.

The SNAP 10A working fluid, NaK 78, precipitates oxides at temperatures in the vicinity of 20°F, with the actual value of temperature being dependent on the impurity content of the NaK. These oxides could cause plugging of the converter tubes, which would hamper system operation. To prevent this, one of the system design specifications is that minimum NaK temperature during this prestartup period be greater than 50°F, giving a safe margin above the expected plugging temperature.

In addition to the minimum temperature specification, a maximum allowed temperature is specified for the prestartup period. This requirement is necessary because various steps in the startup sequence are triggered by the attainment of specified NaK temperatures. The maximum allowed NaK temperature in the prestartup period is 275°F.

Construction features of the ejectable heat shield, and specifications on the eject mechanism, require that temperatures on the shield be held below 350°F. This and the above requirements are met by passive means; i.e., no active heat sources or sinks are used in the system during the prestartup period.

Three factors are effective in ensuring that the above requirements are met. First, the expected ambient temperature of the NPU at the time of launch, greater than 70°F, represents an amount of sensible energy available above the 50°F minimum temperature. Second, battery power supplied to the NaK thermoelectric pump provides a small NaK flowrate during the prestartup period which tends to minimize temperature gradients in the system. A current of 40 amperes will produce a flow about 4% of the design point value. Third, the ejectable heat shield is provided with special emissivity coatings that control the heat transfer between the radiator converter and the space environment to meet the system temperature specifications.

The shield is concentric about the NPU structure, with an annular clearance of about 3/4 in. from the radiators. The basic shield construction consists of an adhesively bonded, aluminum, honeycomb panel approximately 1/4 in. thick. The inside surface is anodized to achieve a low thermal emissivity (about 0.08). The outside is treated with three separate coatings, applied in alternating circumferential stripes, to achieve an overall average thermal emissivity of 0.18 and a solar absorptivity of 0.33.

The operation of these coatings is as follows. The low value of inside emissivity serves to minimize heat loss from the radiator converter to space in the shaded portion of the system. The outside coatings, with the radio of α_S/ϵ greater than one, ensure that a net amount of thermal energy will be absorbed by the system in the region receiving solar energy. As will be seen, the α/ϵ ratio ensures that sufficient solar energy is absorbed to keep the NaK temperature above the allowed minimum value. At the same time, it ensures that enough heat can be rejected at higher temperatures to prevent the maximum temperature specifications from being exceeded.

B. SPACE THERMAL CONDITIONS

There are two principal factors influencing the thermal behavior of the orbiting NPU. First, energy leaving the system by thermal radiation due to its temperature does not return by any reflection mechanism. Space is essentially black. Second, the prime source of energy is that emanating from the sun. This constitutes an energy flux incident on the vehicle of about 443 Btu/hr-ft^2, with this energy being concentrated in the short wave lengths characteristic of the sun's high temperature. For relatively low-altitude orbits, a much smaller additional source of energy is that emanating from the earth, due to its surface temperature (assumed to be 0°F), and that solar energy which is reflected from the earth and incident on the satellite. The SNAP 10A orbital altitude may range from 700 to 3000 mi. At the higher of these orbits, the energy received from the earth becomes negligibly small. As will be seen, the present design adequately meets its design specifications over the entire range of altitudes.

The amount of energy incident on a unit area of the NPU depends on the relative position of the vehicle, the earth, and the sun, as well as the location on the NPU of the area element. The amount of energy leaving the unit area due to its temperature is independent of vehicle location, since none of the emitted

radiation ever returns to the system. The energy leaving for a given temperature is also, to a first approximation, independent of the geometrical location of the area element on the NPU. The net heat entering the element is the difference between the incident and the emitted heat, and is thus a function of vehicle location and position on the surface.

As the system orbits the earth, the relative position of the earth, sun, and NPU may change as a function of time. For example, during a portion of the orbit the NPU may be in the shadow cast by the earth. The changing relative position with time produces a time rate of change of heat input to each area element on the NPU.

The SNAP unit is to be placed in a circular polar orbit from the Pacific Missile Range. Depending on the launch date, the portion of the orbit in which the system is in the shadow of the earth may vary from zero to about 115° (for a 700-mile orbit). Two limiting cases are examined in this analysis. If the line connecting the earth and the sun lies in the NPU orbital plane, the orbit is such as to produce the maximum shade condition described above. This orbit is hereafter referred to as the sun-shade transient orbit. If the earth-sun line is normal to the orbital plane, the system is always in the same position relative to the earth and the sun. In this orbit, one-half of the system is always sunlit and the other half is turned away from the sun. This condition is referred to as the constant sun-constant shade orbit. These two limiting cases are shown in Figure 2.

To predict the thermal behavior of the NPU in the prestartup period, it is necessary to describe mathematically the variation of heat inputs to the system as a function of position on the system and time. The required mathematical derivations are presented in Appendix A. The results are presented in terms of the "effective space temperature." The effective space temperature for a given NPU position and time is the temperature that a black body would require to deliver the same energy to the NPU at that position as is delivered from the sun, both directly and by earth reflection, and from the earth. In addition to the geometrical factors already described, the effective space temperature depends on the solar absorptivity and thermal emissivity of the particular NPU element in question. The effective space temperature is independent of the system temperature at the point in question. The time variation of effective space temperature

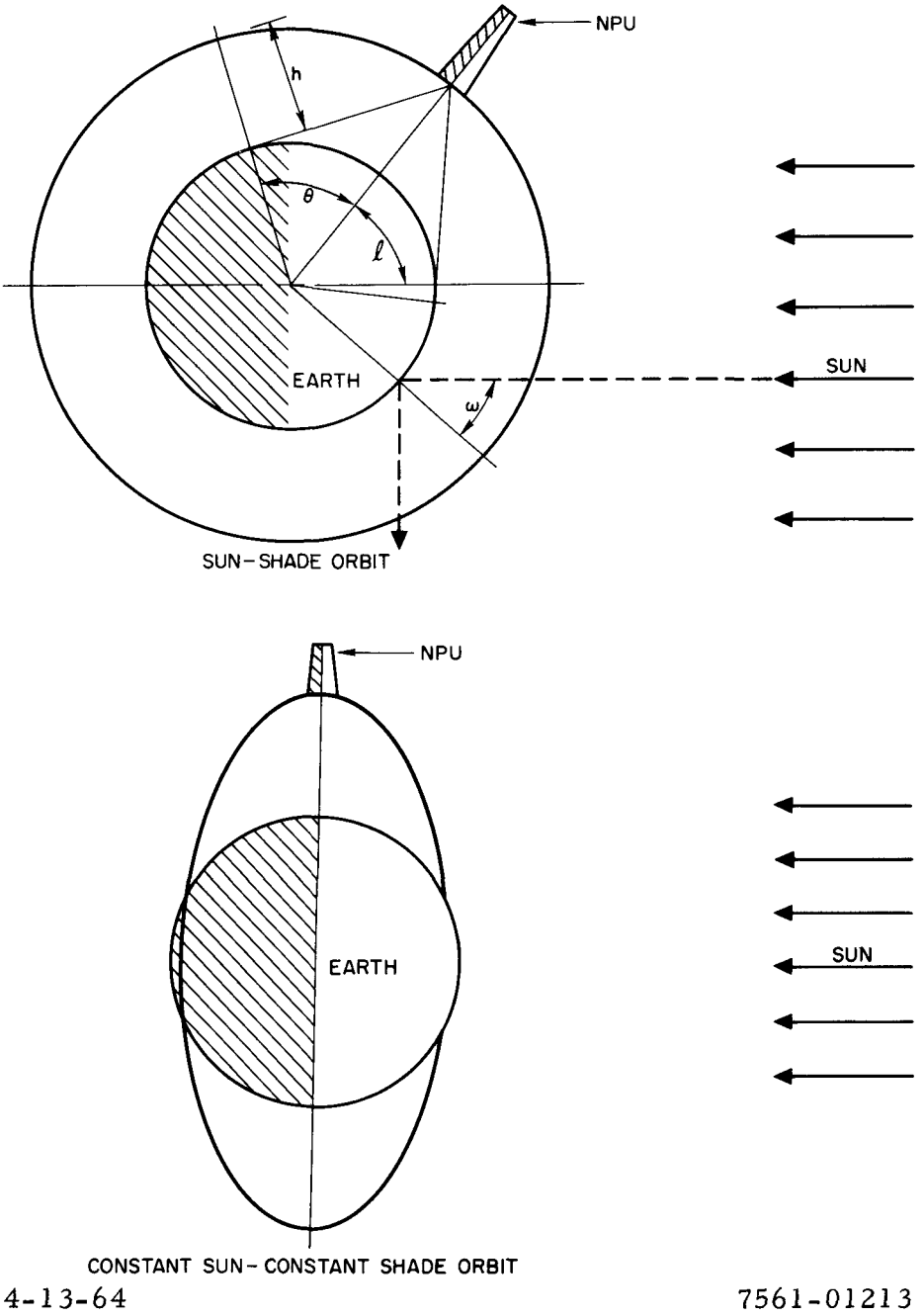

Figure 2. SNAP Unit Orbits

for a typical point on the heat shield in the 700-mile sun-shade transient orbit is shown in Figure 3.

Since the relative position of NPU, earth, and sun is independent of time in the constant sun-constant shade orbit, the effective space temperature is also independent of time. The value of effective space temperature under these

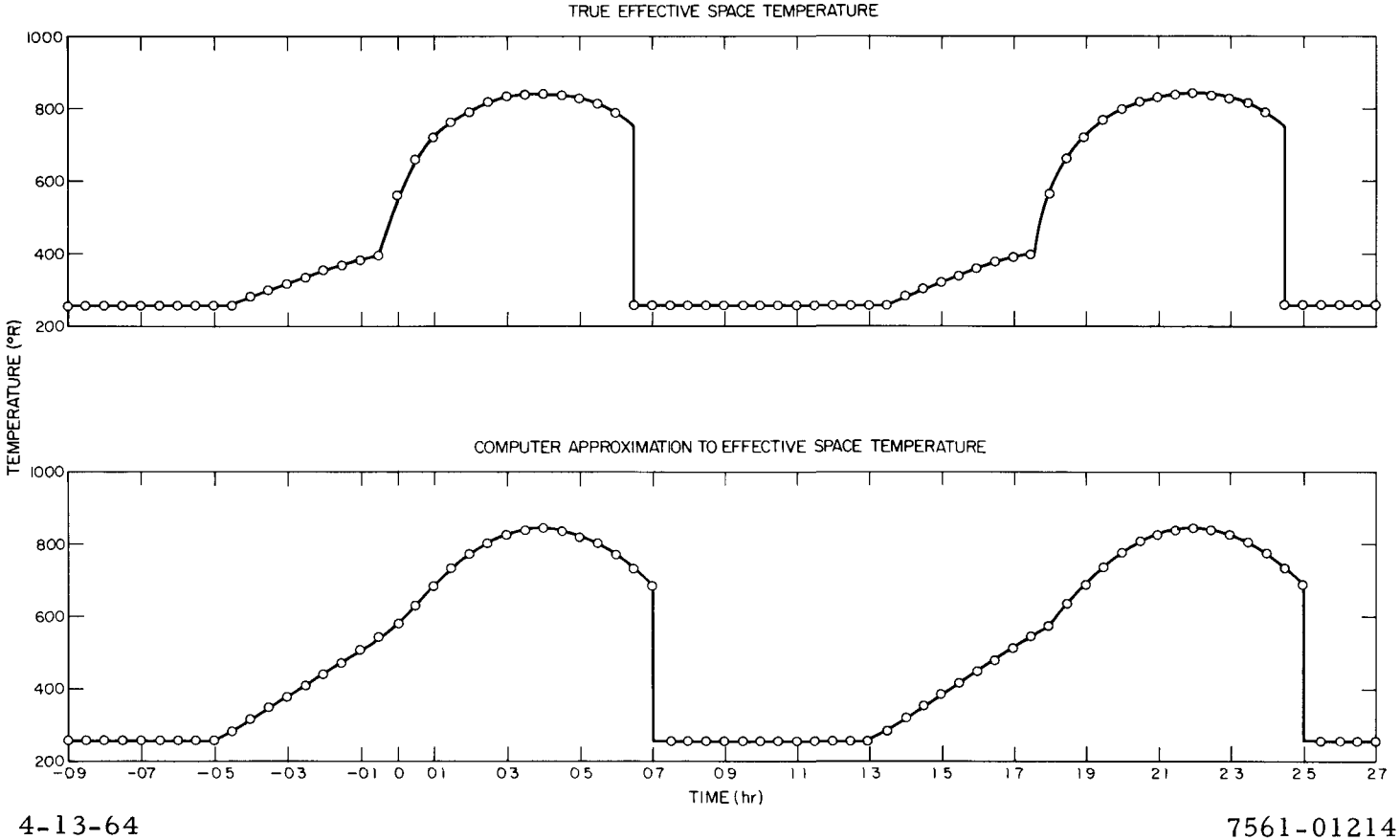

Figure 3. Time Variation of Effective Space Temperature, Heat Shield Node 314

conditions corresponds to the value taken on in the sun-shade transient case when the system is over the poles. This corresponds to the value at time = 0.45 hr for the point corresponding to Figure 3.

C. SYSTEM THERMAL MODEL

It is now possible to state the problem of predicting the prestartup thermal behavior in a general way. It is necessary to predict the temperature variations in position (on the NPU) and time, from an initial temperature distribution, under a time-varying heat supply rate. In particular it must be shown that all the temperature requirements of Section III-A are met.

The problem of describing temperature variations with position on the NPU is handled by dividing the various system components into a series of "lumps" or "nodes" which are assumed to be of uniform temperature throughout. An energy balance is then made on each of these nodes that describes the heat inflow and outflow to the node by the appropriate heat transfer mechanism. The net heat inflow represents an instantaneous rate of accumulation of energy in the node, which may be related to the rate of change of the node temperature. Thus, the energy balance takes the form of an ordinary, nonlinear differential equation in the node temperature, with time as the independent variable.

The mathematical derivation of the equations described above is presented in Appendix A. All three of the important modes of heat transfer, namely conduction, bulk transport or convection, and radiation, play a role in this derivation. The effective space temperature as seen by the external nodes of the system play the role of "forcing functions" in the set of differential equations. The principal source of nonlinearity in the equations is the dependence of radiative transfer on the fourth power of system temperatures. Other potential sources of nonlinearity, such as dependence of material properties (heat capacity, conductivity) on temperature, have been neglected.

As the NPU orbits the earth, the solar heating is always symmetric about a plane through the SNAP long axis and parallel to the earth-sun line. In the constant sun-constant shade orbit, this plane is determined by the vehicle yaw and pitch axes. In the sun-shade transient orbit, the plane is determined by the vehicle yaw and roll axes. In both cases, the plane is also a plane of symmetry for the NPU. Therefore, if attention is restricted to initial conditions which are

symmetric, it is only necessary to provide nodes for one-half of the system, the temperatures of the other half being available by application of the symmetry condition.

To permit a detailed description of the variation of temperature with position on the power unit, the one-half modeled was divided into 270 nodes distributed on the system as shown in Table 2. An additional 76 nodes are required to describe the thermal environment. The description of the prestartup thermal behavior involves the solution of this 270th order set of ordinary differential equations. This system of equations was solved numerically by converting the differential equations into difference equations in time, and solving these equations stepwise from the initial conditions on a digital computer. The IBM 7090 computer was used, and the computation time required was of the order of 100th the real time simulated.

TABLE 2

SIMULATION NODE BREAKDOWN

Component	Number of Nodes
Reactor	1
Reflector	1
Pump	4
Neutron Shield	24
Structure	60
NaK Tubes	54
Radiator	54
Heat Shield	72
Space Temperature	76

D. COMPARISON OF MODEL WITH TEST DATA

To provide a check on the assumptions used in modeling the system, the computer code was checked against actual ground test data. The data used were obtained from the Prestartup Orbital Operations portion of the System Test on Flight System Mockup-1 (FSM-1). The FSM-1 is a duplication of the SNAP 10A flight system in all respects, except that the nuclear core is replaced by an electrical heater capable of the same heat generation as the actual core.

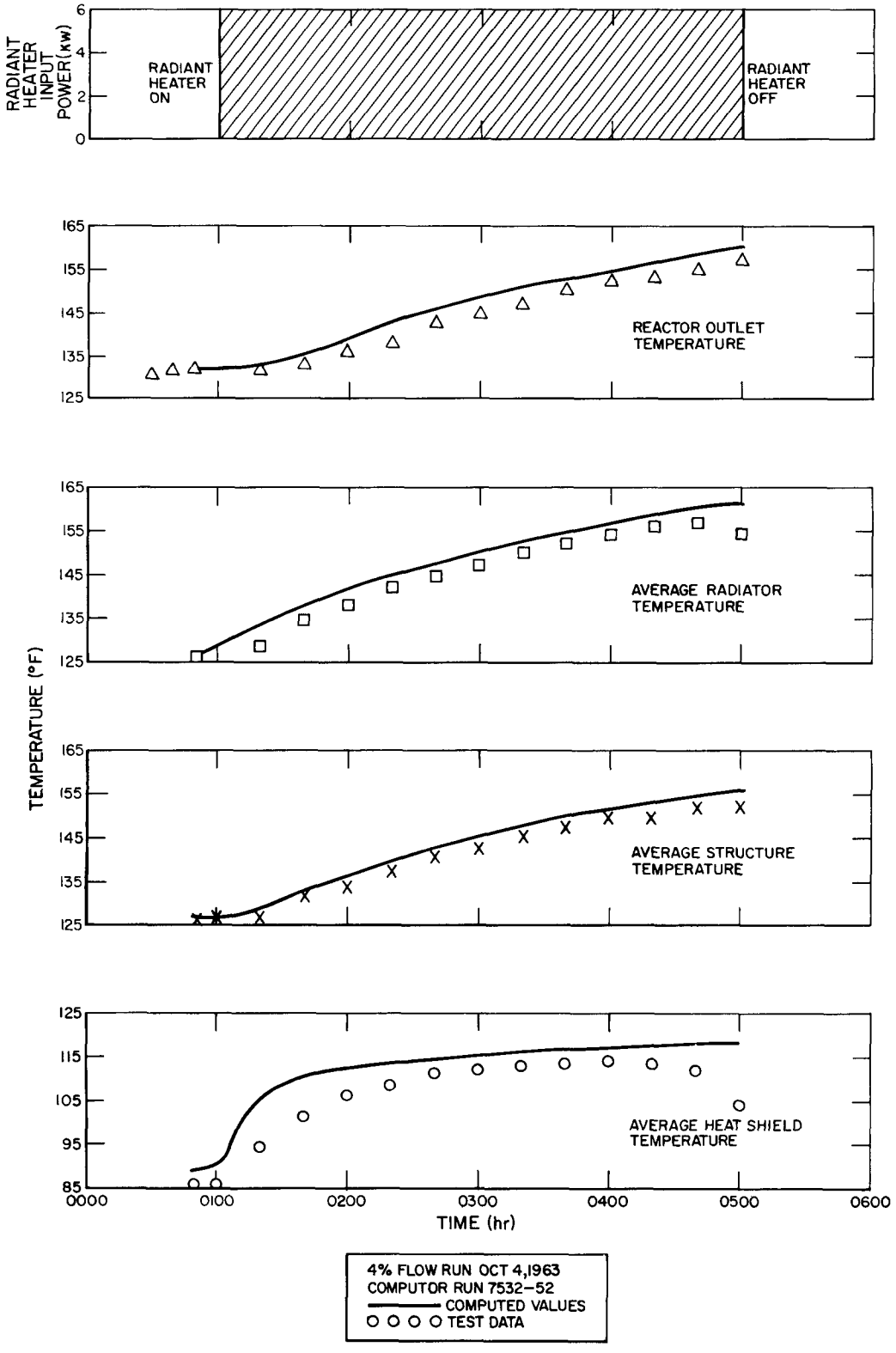

4-13-64 7561-01215

Figure 4. Comparison of Computer Model Results With Test Data, FSM-1

The system test was conducted in a vacuum vessel outfitted with radiant heat lamps to simulate the solar heat input. The FSM-1 system is instrumented with standard flight instrumentation, as well as special instrumentation to provide a detailed record of system performance. This instrumentation is connected to a data logger which recorded test results at 10-min intervals.

The FSM-1 Prestartup Orbital Operations test was not intended to predict temperatures under actual space conditions, since the environmental equipment available failed to duplicate space conditions in a number of respects. Rather, the intent was to test the system thermal behavior under known conditions in the low-temperature range expected in space. As will be shown below, this known test environment could be entered into the computer model of the system, in an attempt to duplicate test results with the model.

The test procedure used was to allow the system to reach thermal equilibrium in the vacuum vessel, then to turn on the radiant heaters along one side of the vacuum vessel to simulate the constant sun-constant shade environment. The lamps were left on for a period of 3.6 hr, corresponding to two orbits at 600-mile orbital altitude.

The temperature histories of certain key variables, as obtained from the computer model, are presented in Figure 4, together with data points obtained from the FSM-1 test. The run shown corresponds to a system flowrate of 4% of design. As can be seen from the figure, there is substantial agreement between the computed results and the test data.

A detailed comparison of the computed and measured system temperatures is given in Figures 5 through 8. The temperatures shown correspond to the end of the test; i.e., after the lamps have been on for 3.6 hr. As can be seen, the basic computer grid represents a detailed description of the spacial variation of temperatures. The test values have been located on the diagram in the position which corresponds to their actual location on the system. The agreement again is good, and this comparison is taken as adequate justification for the assumptions used in preparing the model.

A test is planned for the near future in which improved environmental equipment will be available. It is expected that this test will provide system temperatures very close to those predicted for the actual space environment.

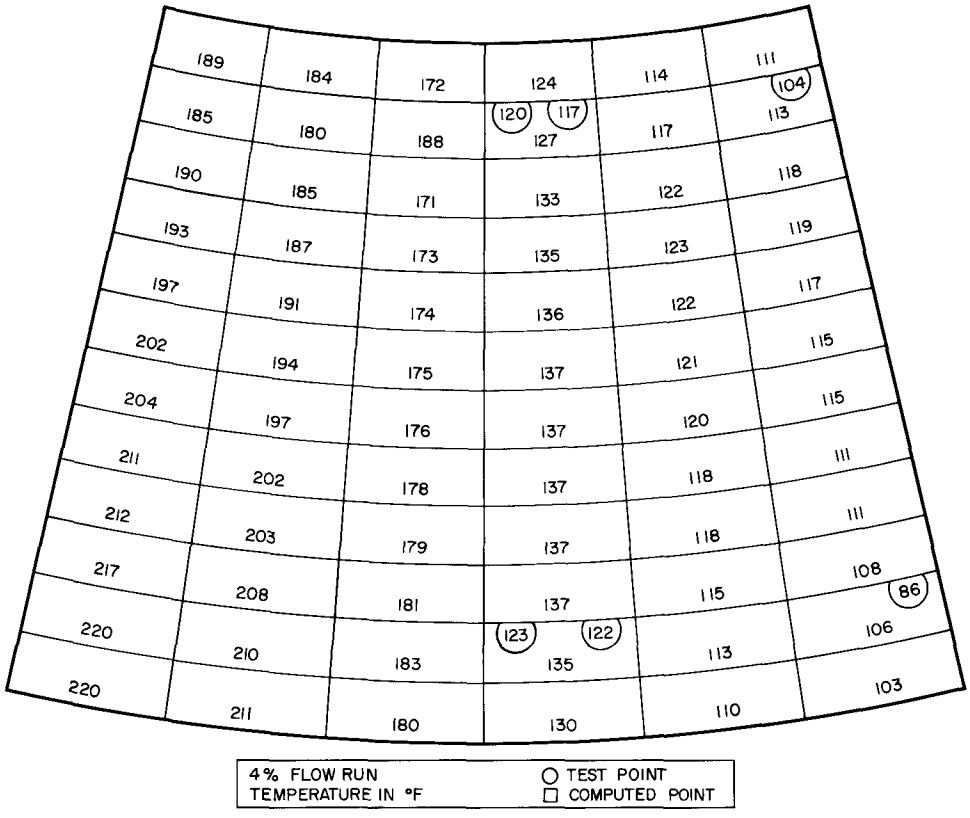

4-13-64 7561-01216

Figure 5. Comparison of Test Data and Computer Results, Heat Shield Final Conditions

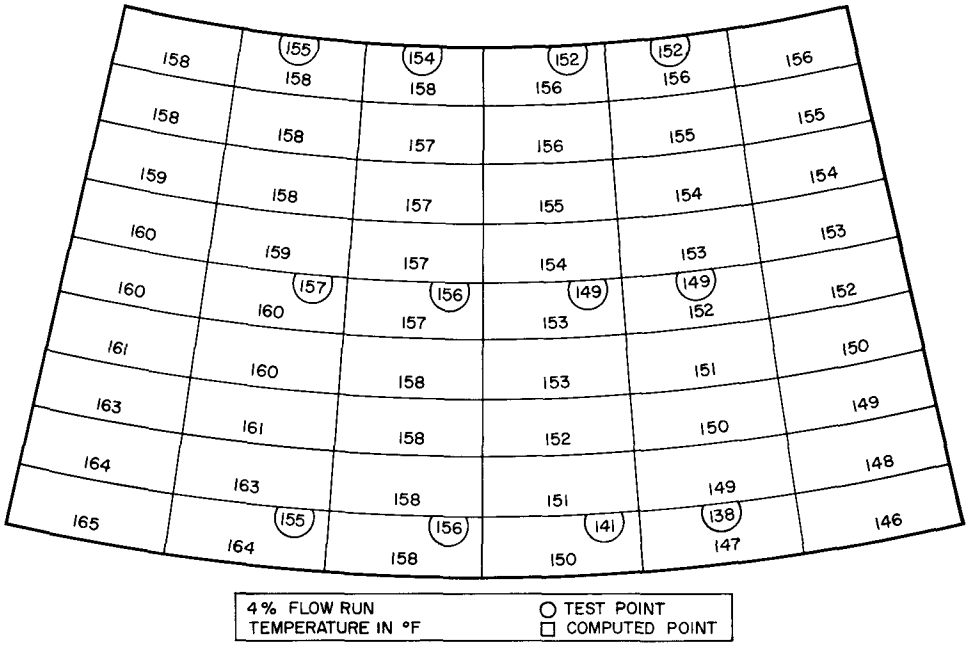

4-13-64 7561-01217

Figure 6. Comparison of Test Data and Computer Results, Radiator Final Conditions

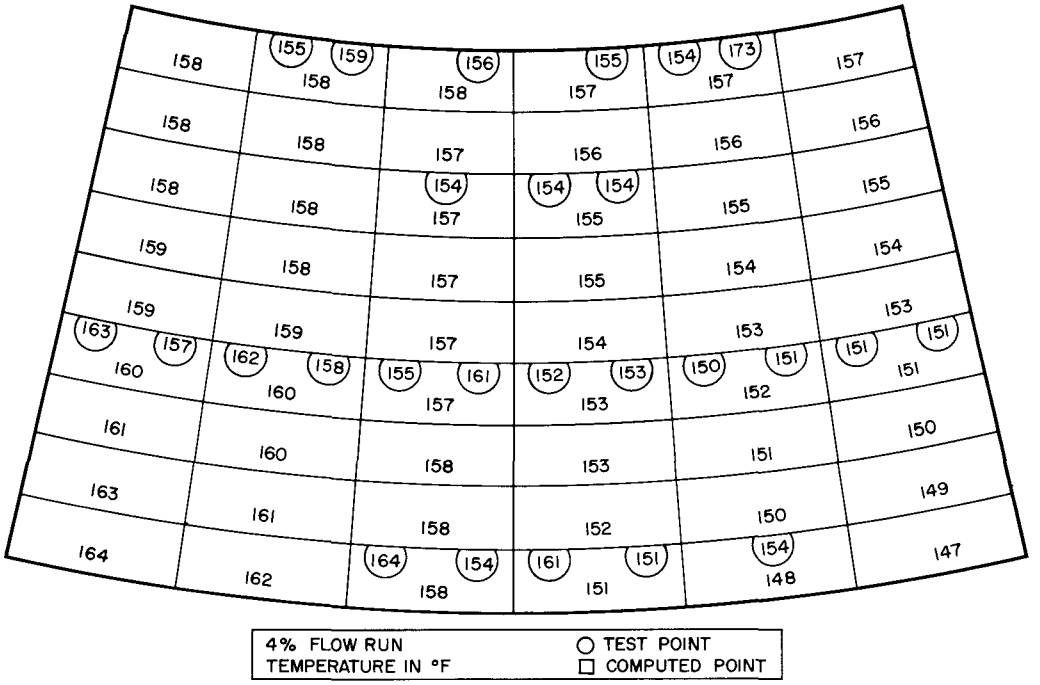

4-13-64 7561-01218

Figure 7. Comparison of Test Data and Computer Results, NaK Tube Final Conditions

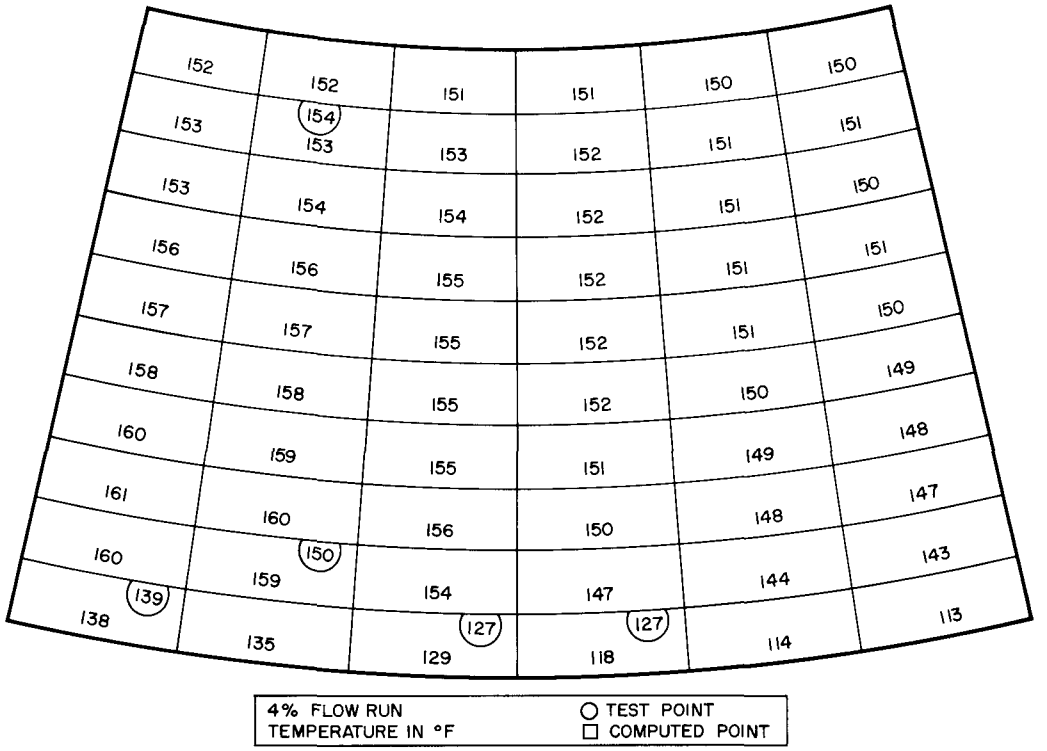

4-13-64 7561-01219

Figure 8. Comparison of Test Data and Computer Results, Structure Final Conditions

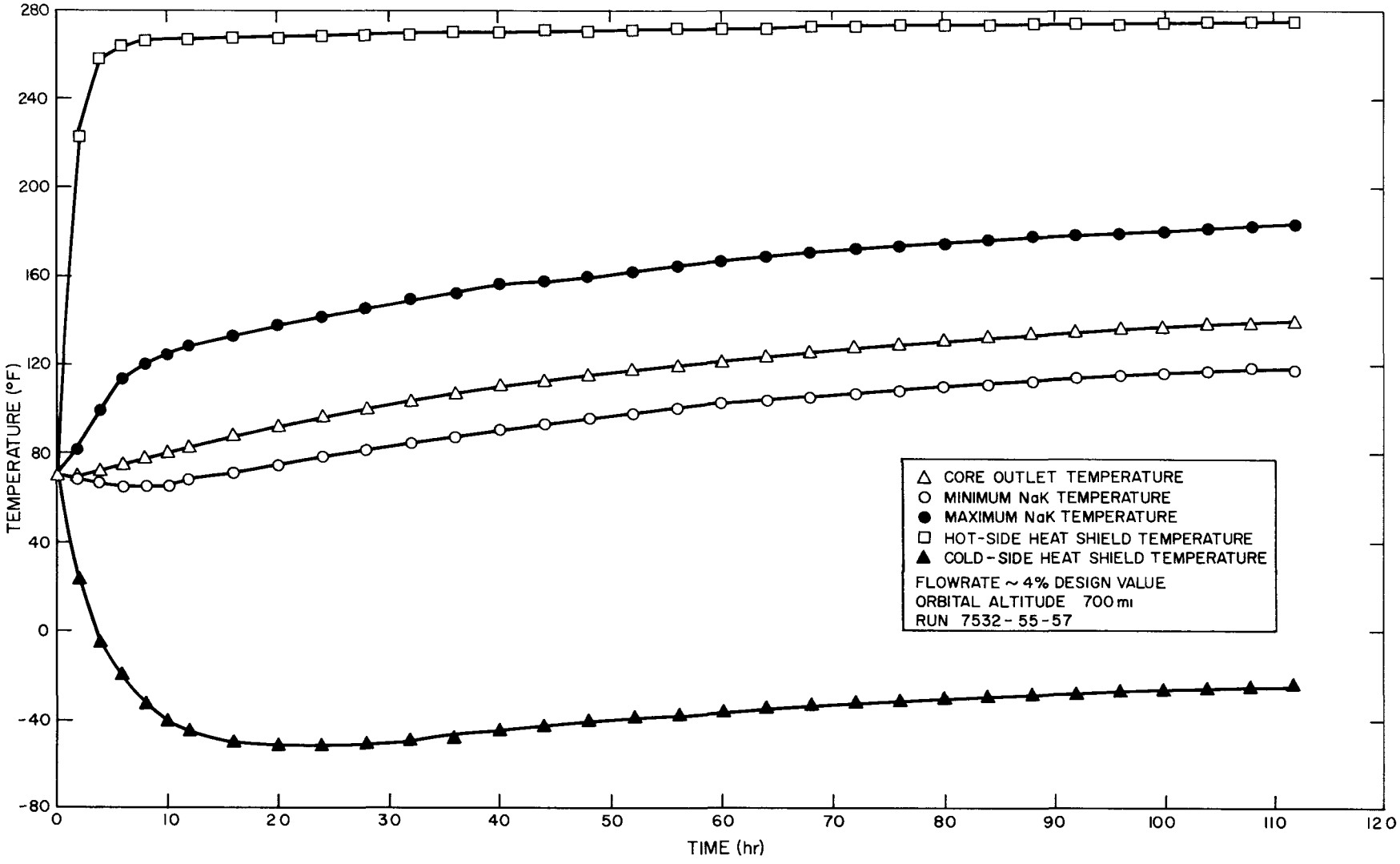

4-13-64 7561-01220

Figure 9. SNAP 10A Prestartup Orbital Analysis, Constant Sun-Constant Shade Orbit

E. DESCRIPTION OF RESULTS

The results of the model described in Sections III-B and III-C are discussed in this section and compared with the requirements of Section III-A. The base case selected is a 700-mile orbit with the coefficients in the system equations evaluated at design values of thermal properties. A flowrate of 4% of the design operating value is assumed to be supplied by the pump. Both constant sun-constant shade, and sun-shade transient orbits are discussed.

The basic temperature histories for the constant sun-constant shade orbit, run from a constant 70°F initial temperature, are shown in Figure 9. The figure covers a duration of about six orbits (orbital period equals 1.8 hr). As can be seen from the figure, the minimum NaK temperature occurs in the first orbit and is well above the 50°F minimum allowable. The core outlet temperature, given by the central curve of the figure, is undergoing a slow rate of increase of temperature. This temperature is approaching a value very near the fourth power average of all the effective space temperatures seen by the system. It is this rise of core outlet temperature which eventually catches the falling NaK temperature on the cold side and carries it upward. The extreme temperatures shown in the figure are the average hot- and cold-side temperatures of the heat shield. The heat shield rapidly attains a pseudo-equilibrium temperature, in which it is essentially in equilibrium with the existing NaK temperature in the converter and the effective space temperature. Thereafter, it undergoes a slow variation as the converter-radiator temperature rises. Over the time period shown, the slow rate of response of the core outlet temperature is a consequence of the high resistance to heat transfer presented to the space environment by the heat shield. This is principally due to the low value of inside emissivity. The tendency for the temperature to rise rather than fall is a consequence of the favorable ratio of solar absorptivity to thermal emissivity used on the outside of the heat shield.

The temperature distributions throughout the NPU at equilibrium in the constant sun-constant shade orbit are shown in Figures 10 through 16. These figures also serve to illustrate the degree of detail which has been used in simulating the system. The effective space temperatures are included in the figures. Comparison of the effective space temperatures (Figure 10), the heat shield temperatures (Figure 11), and the radiator temperatures (Figure 12), shows how the heat shield serves to "soften" the severe temperature gradients imposed

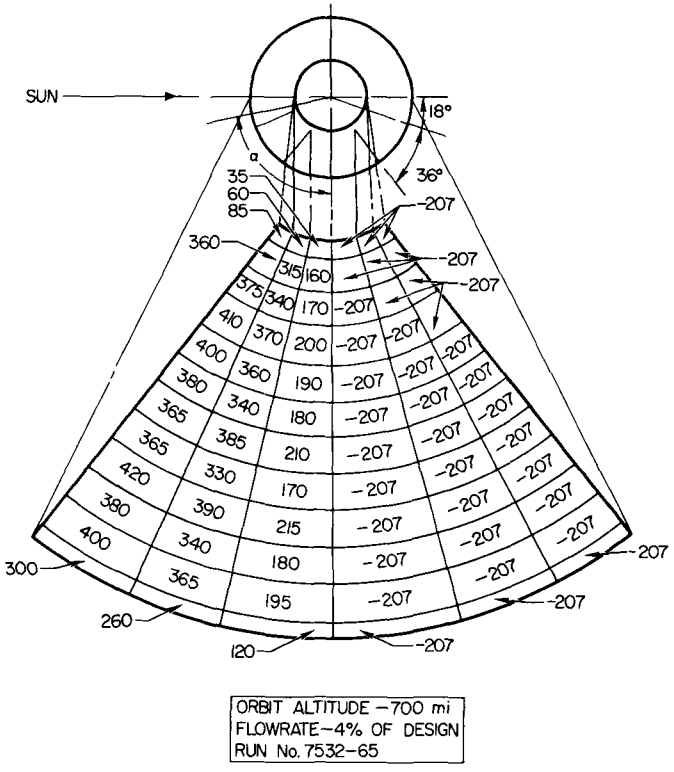

4-13-64 7561-01221

Figure 10. Effective Space Temperature Distribution (°F), Constant Sun-Constant Shade Orbit

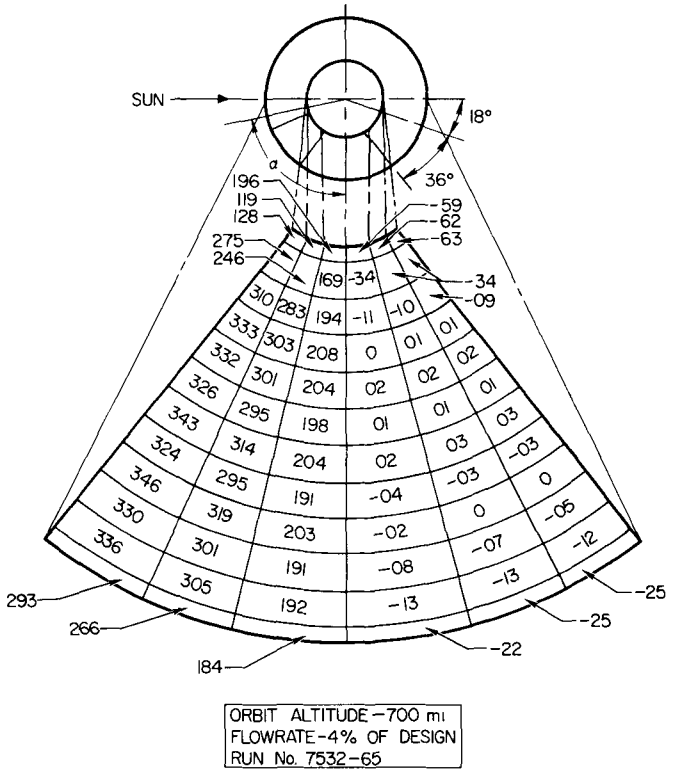

Figure 11. Heat Shield Equilibrium Temperature Distribution (°F), Constant Sun-Constant Shade Orbit

4-13-64 7561-01222

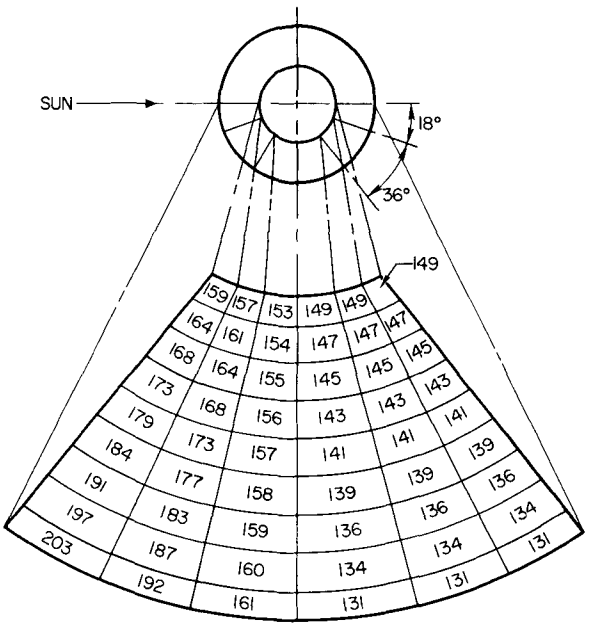

4-13-64 7561-01223

Figure 12. Radiator Equilibrium Temperature Distribution (°F), Constant Sun-Constant Shade Orbit

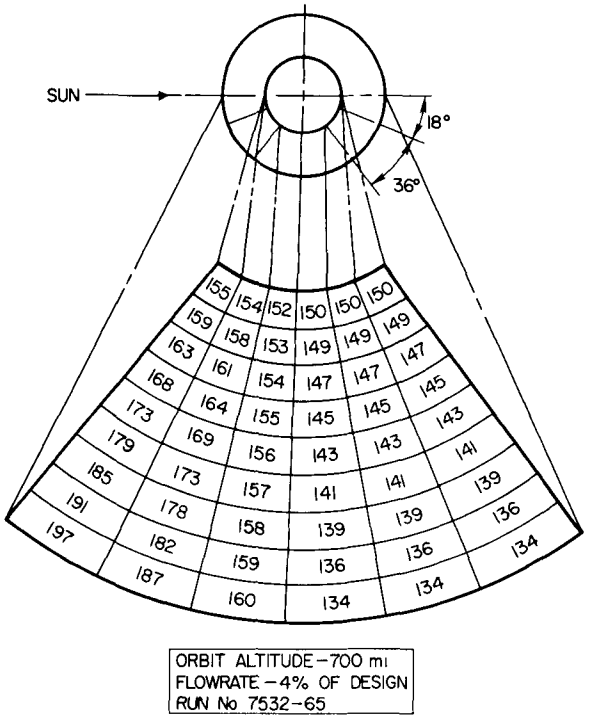

4-13-64 7561-01224

Figure 13. NaK Tube Equilibrium Temperature Distribution (°F), Constant Sun-Constant Shade Orbit

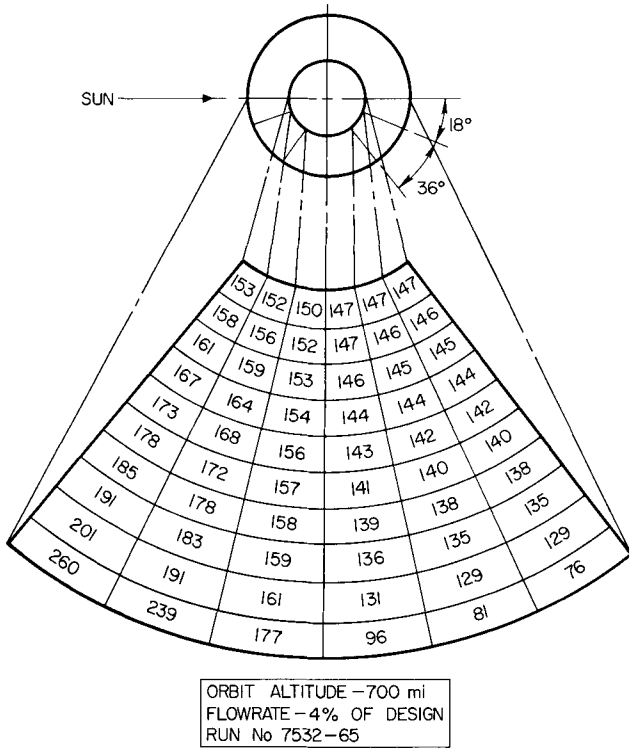

4-13-64 7561-01225

Figure 14. Structure Equilibrium Temperature Distribution (°F), Constant Sun-Constant Shade Orbit

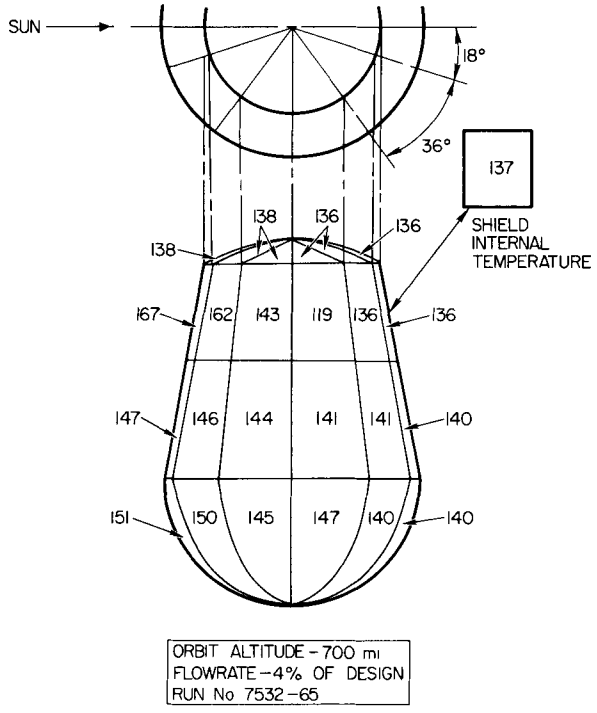

4-13-64 7561-01226

Figure 15. Neutron Shield Case Equilibrium Temperature Distribution (°F), Constant Sun-Constant Shade Orbit

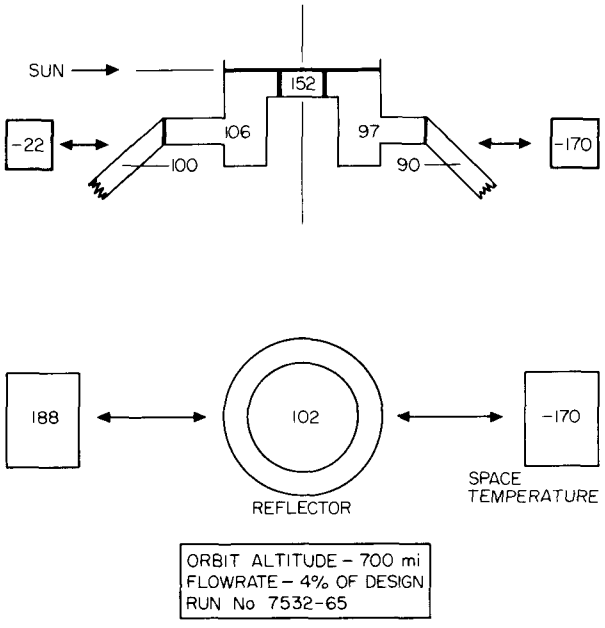

4-13-64 7561-01227

Figure 16. Pump and Reflector Temperature Distribution (°F), Constant Sun-Constant Shade Orbit

upon the NPU by the space environment. Thus, a 600°F circumferential variation space temperature is reduced to a 350°F variation on the heat shield and a 40°F variation on the radiator. It can be seen also that the maximum temperature on the heat shield and the maximum NaK temperature are within the allowed values. Since the constant sun-constant shade orbit produces the maximum temperatures, this result verifies that the design meets the maximum temperature requirements.

Temperature histories for the sun-shade transient orbit are shown in Figures 17 and 18. The minimum NaK temperature in this orbit is 61°F (not shown) which is slightly lower than that in the constant sun-constant shade case, but still well above the minimum allowable. The minimum is again reached in the first orbit. The initial latitude in the sun-shade transient orbit was selected to produce a "worst-case" condition; i.e., the starting point shown is the one which produces the lowest minimum NaK temperature. This corresponds roughly to the "launch-site shade" condition. The apparently slower rate of heatup of reactor temperature is due to the fact that the equilibrium temperature to which it is going is substantially lower in the transient orbit than in the constant

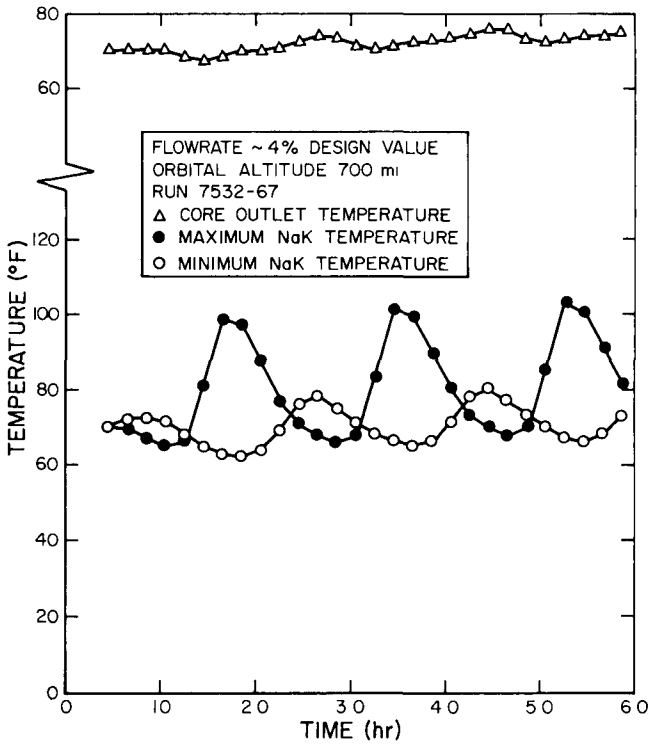

4-13-64 7561-01228

Figure 17. SNAP 10A Prestartup Orbital Analysis, Sun-Shade Transient Test (2/18/64)

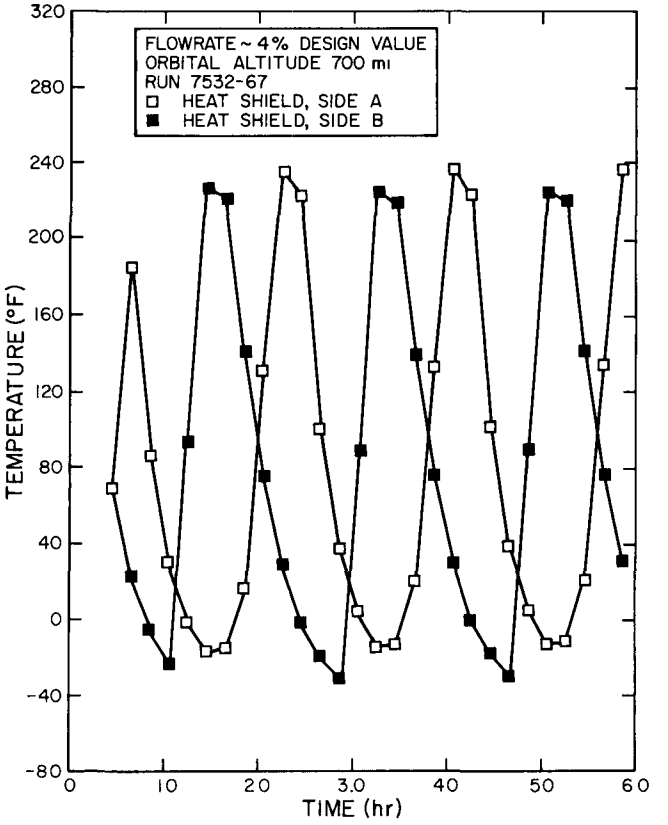

4-13-64 7561-01229

Figure 18. SNAP 10A Prestartup Orbital Analysis, Sun-Shade Transient Test (2/11/64)

sun-constant shade orbit. The overall nature of the system response is that of a small temperature oscillation superimposed on a slow rise. Comparison of the heat shield response (Figure 18) with that of the core outlet temperature (Figure 17) again shows the attenuation introduced by the presence of the heat shield.

F. EFFECTS OF PARAMETER VARIATIONS

In the preceding section it was shown that all system thermal requirements are met when system parameters take on their design values. In this section, the effects on performance of small variations in system parameters are discussed. The effects considered are changes in prestartup flowrate, orbital altitude, heat shield solar absorptivity (α_S), outside thermal emissivity (ϵ_O), and inside emissivity (ϵ_i). Qualitative aspects of the procedures used are discussed and the results presented in this section. Pertinent derivations are included in Appendix A.

First to be considered is the effect on minimum NaK temperature of changes in the prestartup flowrate. This flowrate could change from the expected value of 4% of design flow because of changes in the battery current supplied to the pump or a change in pump properties. It has been shown that the minimum NaK temperature occurs in the first orbit. It is to be expected that a decrease in the flowrate will cause the minimum to be lower and of longer duration. These qualitative conclusions have been quantitatively tested by repeating the computer simulations at two lower flowrates. Plots of the minimum NaK temperature as a function of flowrate are given in Figure 19. The minimum temperature is seen to be insensitive to flowrate in the sun-shade transient orbit, but in the constant sun-constant shade test it becomes increasingly sensitive as the flowrate is reduced. In Figure 20, the length of time from launch to the time when the minimum NaK temperature occurred is plotted as a function of flowrate. Again, the sun-shade orbit results are relatively insensitive to flowrate, while the constant sun-constant shade orbit becomes sensitive at low flows. It is concluded from these results that an adequate margin of safety is available to ensure that the 50°F minimum temperature specification will be met.

The second consideration is that of the effects on minimum NaK temperature of changes in orbital altitude. In the constant sun-constant shade orbit, the effect of increasing the orbital altitude is to decrease the amount of thermal energy

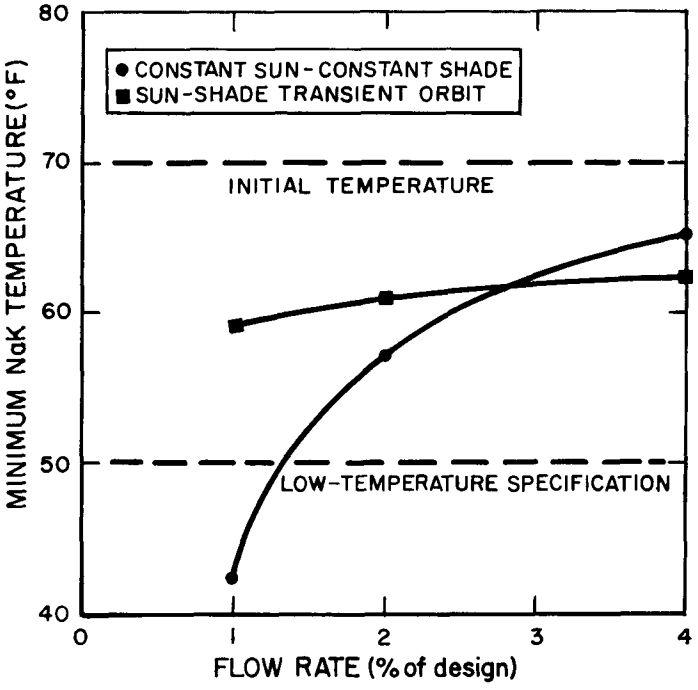

4-20-64 7561-01230

Figure 19. Effect of Flowrate on Minimum NaK Temperature

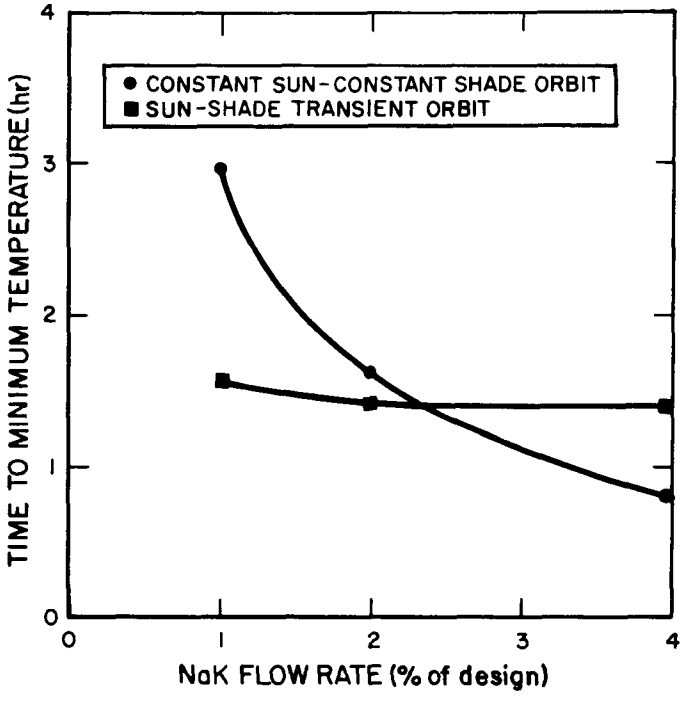

4-20-64 7561-01231

Figure 20. Effect of Flowrate on Time to Minimum Temperature

reaching the NPU from the earth. This is due to the fact that the view factor from earth to satellite decreases rapidly as the orbital altitude increases. At an altitude of 3000 miles the energy received from the earth is down by a factor of 10 from that at 700 miles. Fortunately, the fraction of total energy that is received from the earth is small (about 5% at 700 miles). In the sun-shade transient orbit, this loss is offset by the fact that the fraction of the orbital period spent in the earth's shadow decreases rapidly. The actual time spent in the shade increases very slightly, but the orbital period increases rapidly. Thus, the undesirable effects of orbital altitude are most pronounced in the constant sun-constant shade orbit.

Also to be considered is the effect on minimum NaK temperature of changes in the heat shield thermal properties, α_S, ϵ_O, and ϵ_i. These parameters are subject to a variation of ±10% about their mean values. The worst situation with respect to minimum NaK temperature results from a combined decrease in α_S and an increase in ϵ_i and ϵ_O. This causes a decrease in the solar heat absorption rate and an increase in the rate of thermal losses from the NPU. For computational purposes, it is convenient to translate these changes into equivalent changes in effective space temperatures, combine these with changes in space temperatures equivalent to a change in orbital altitude, and then use a single computer run to evaluate this combined worst case.

In seeking the equivalence between changes in thermal properties and changes in space temperatures, the objective is to cause the same change in net heat leaving the converter in the time period corresponding to the first few orbits. Use was made of the fact that the converter temperature will be near the launch temperature (70°) and the heat shield will rapidly reach a pseudo-equilibrium with the converter and space.

The simulation used to study these effects consisted of the same model used in the base case constant sun-constant shade run with modified space temperatures. A cold-side temperature of 0°F was used, rather than 253°R. A constant-sun-side space temperature of 720°R was used in place of a space-varying distribution with an average temperature of 750°R. The system temperature responses as a function of time are shown in Figure 21. A comparison with Figure 14, the base case, shows that the minimum temperature is slightly lower and the rate of recovery and increase is slower. However, the overall behavior is well within the specification.

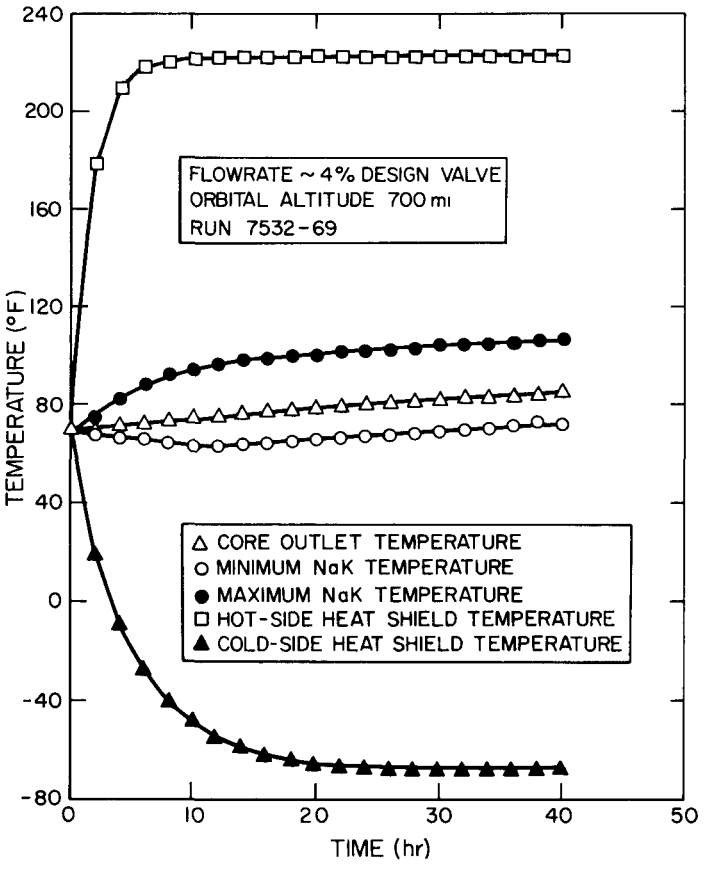

Figure 21. SNAP 10A Prestartup Orbital Analysis, Constant Sun-Constant Shade Orbit, Worst Case Thermal Environment (2/14/64)

The third case to consider is the effect of changes in the heat shield thermal properties on the maximum temperature of the heat shield. There is no need to consider changes in orbital altitude, since the 700-mile orbit is already the worst case in this regard. The worst case change in thermal properties in this case is the reverse of that which was worst in the case of minimum NaK temperature. This corresponds to an increase in α_S and decreases in ϵ_i and ϵ_o. This maximizes the solar heat absorption and minimizes the thermal heat loss rate. Further, the worst situation occurs at equilibrium rather than near the launch time. The size of the effect was estimated by a steady-state heat balance which computed the change in average heat shield temperature due to the change in heat shield properties. This change is then assumed to hold at all points, and the new maximum temperature becomes the old maximum from Figure 11 plus the

calculated increment. This analysis predicts a worst-case maximum heat shield temperature of 385°F. This value exceeds the specified maximum of 350°F. This analysis also provides an estimate of the maximum core outlet temperature. The predicted value is 176°F, which is well within the 275°F specified maximum value.

BLANK

IV. STARTUP ANALYSIS SECTION

A. STARTUP AND CONTROL REQUIREMENTS

Upon confirmation of a long-life orbit, a signal from the vehicle ground command system starts the active control phase. At this time, the system is in a subcritical state with a temperature distribution determined by the space environment.

The primary requirement of the startup and control system is to bring the NPU from this subcritical low-temperature state to criticality, sensible heat generation, initial operating conditions, and finally to stabilized operating conditions. In addition to the primary requirement, the following requirements also must be met.

1) The system must be brought to rated operating conditions in such a manner that the resultant startup transients do not impose thermal shocks, stresses, or temperatures that would jeopardize system integrity.

2) The system must operate in a stable manner to minimize thermal cycling of the system and controller component wear.

B. STARTUP AND CONTROL SYSTEM DEVELOPMENT

The static nature of the thermoelectric power converter and pump reduces remote automatic startup to a problem of reactor startup alone. The major operation is to achieve criticality and rated power and temperature conditions for the reactor. The power conversion system and coolant flowrate automatically approach rated conditions as the reactor outlet temperature approaches its rated value.

To bring the reactor to rated power and temperature from its initial cold subcritical state, it is necessary to insert reactivity to bring the reactor to the critical state. Reactivity insertion is also required to overcome the negative reactivity defect introduced by core temperature increase. This is accomplished by inward rotation of control drums located in the reflector.

Initial startup of a nuclear reactor is usually accomplished in a very cautious manner. Great reliance is placed on nuclear instrumentation to determine

the precise location of criticality. After criticality is attained, the operator brings the reactor to rated power on a slow period by observing the neutron flux and period instruments and by making the necessary changes.

Clearly, the method just described cannot be duplicated in an automatic startup in orbit unless a complex system of instrumentation and sophisticated feedback controls is used. The guiding philosophy of high reliability, which is attendant with simplicity, makes it inadvisable to devise a reactor startup control system using nuclear measurements as feedback signals. Rather, it indicates that programmed reactivity insertion during startup be utilized with temperature feedback control employed only for establishment of initial operating conditions.

The control system is further simplified by use of a unilateral control mode. Unilateral control is herein defined as regulation of a variable in only one direction. With respect to the SNAP 10A system, the variable is reactor outlet temperature and the direction of regulation is increasing temperature. The unilateral control mode is possible for the following reasons:

1) The SNAP 10A mission objectives do not require, at any time, a shutdown or dropping of reactor power by the control system. Therefore, it is only necessary to insert reactivity, and this can be done with a unilateral controller.

2) Fortunately, the SNAP-type reactors are highly self-stabilizing. This is due primarily to the relatively large, negative temperature coefficients.

3) The possibility of any unforeseen reactor or system effects which would increase reactor outlet temperature beyond tolerable limits has been shown to be negligibly small. Therefore, a control system capable of reducing reactor outlet temperature is not required.

4) The use of a unilateral control system has the obvious advantage of simplicity, and it eliminates the possibility of unstable limit cycling involving the controller.

C. ANALYSIS OBJECTIVES

As a result of the preliminary design studies, the present simple startup and control method has evolved. Briefly, this method consists of insertion of

reactivity at an average constant rate until the reactor outlet temperature attains a preset value. The control system will be described in greater detail later in the report. Subsequent analyses, using the best available analytical and test data, have demonstrated the feasibility of this method of startup in meeting the primary requirement.

However, changes have occurred in system parameters in the evolution of the NPU to its present state. Although the basic startup and control method remains the same, a reevaluation of the system dynamic behavior during startup was made. This analysis included the latest system parameters.

The analysis objectives were twofold. The first objective was to predict typical startup transient histories such as reactor power, temperatures, coolant flow, etc. This information was then used to determine both flight and ground-test system performance criteria during the startup phase. Of equal importance, this information has been used in subsequent studies to determine if the startup transients impose any thermal shocks, stress, or temperatures greater than design allowances. The second analysis objective was to determine parameter sensitivity; i.e., to determine the effect on the startup transients of variations of critical system parameters from their nominal values. The results of the parameter study phase of the analysis were then used to determine if the range of parameter variations could jeopardize system integrity.

D. DESCRIPTION OF STARTUP AND CONTROL SYSTEM

The following is a description of the startup and control system components and operation. The relationships of the components are shown in Figure 22.

1. Temperature Sensor Switch

The temperature sensor switch performs three functions. First, it senses the reactor outlet temperature. Second, it compares the sensed temperature to the set point value (i.e., reference temperature). Third, it provides a binary error signal to the controller. The error signal characteristic is presented in Figure 23. The sensor location is on the reactor outlet line just above the pump. Two temperature sensor switches are connected in parallel to increase the control system reliability.

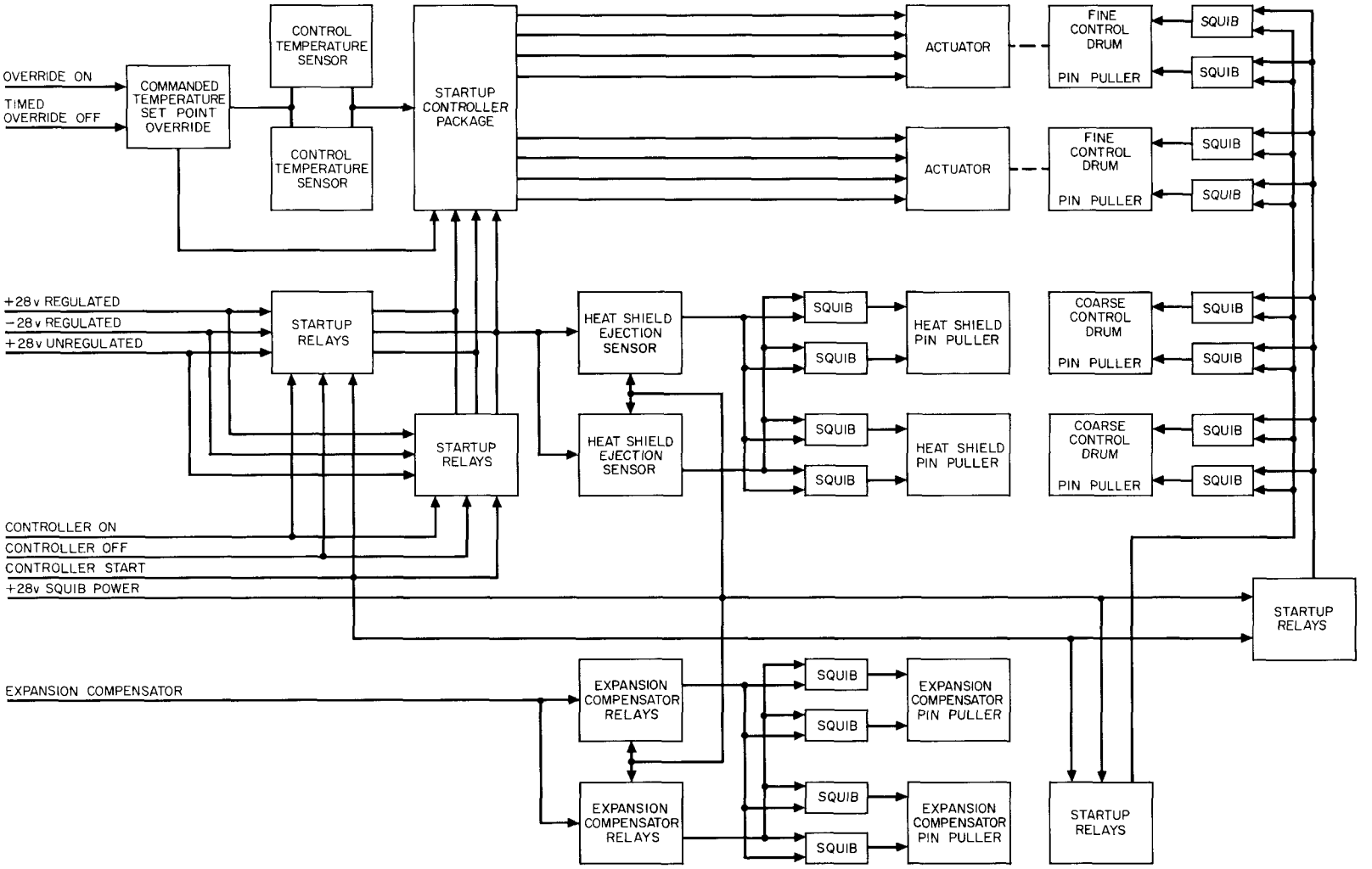

4-13-64

7561-01233

Figure 22. Startup and Control System Block Diagram

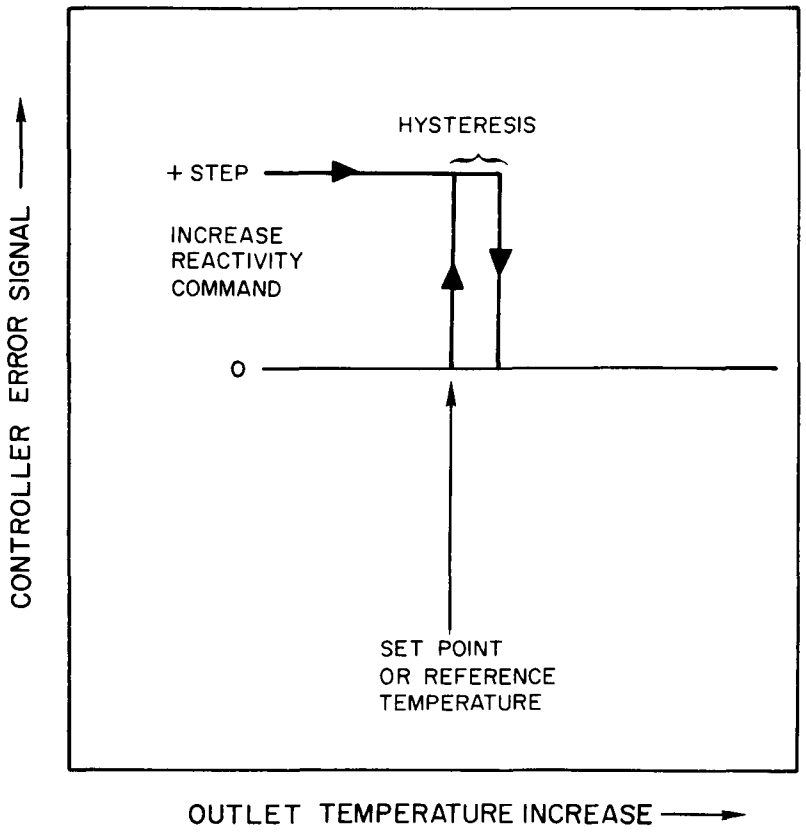

Figure 23. Controller Error Signal Characteristic

2. Startup Controller Package

The startup controller package contains the circuitry and hardware necessary to provide periodic pulses of power to the control drum actuators. Upon receipt of an error signal from the temperature sensor switch, the periodic sequence of power pulses to the drum actuators is started and continues until the error signal ceases or the control system is commanded off. The period of the pulse sequence determines the drum stepping rate.

3. Actuator Drums

The reactor assembly has a total of four control drums located in the reflector. These drums supply the reactivity to bring the reactor from a subcritical to full power condition. Two of the drums are designated coarse control drums and the other two, fine control drums. Each drum is worth approximately $2.40. Figure 24 shows the drum-worth position relationship. The two coarse control drums are inserted rapidly upon startup command by means of preloaded

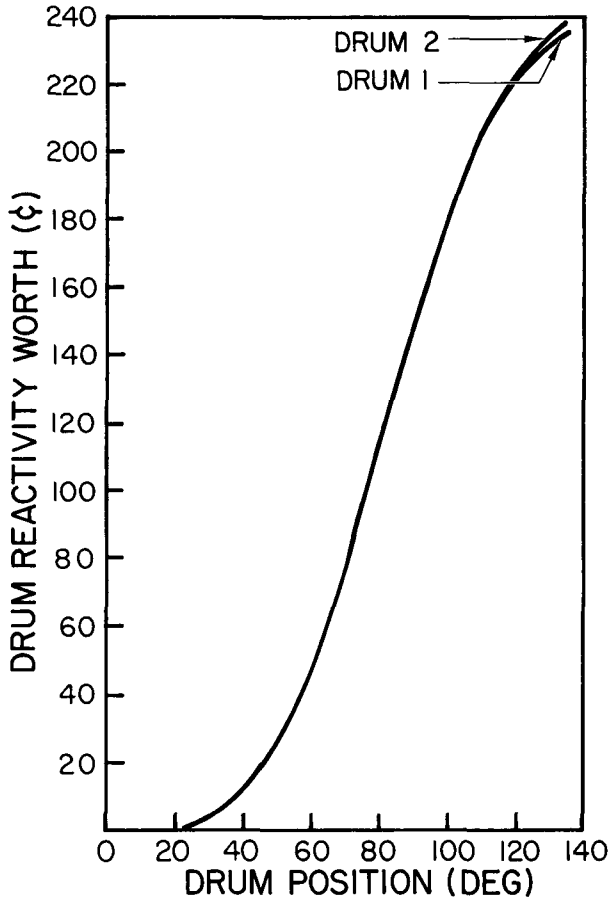

Figure 24. Drum-Worth Position Relationship, 1 Shim Case

springs. The insertion of the coarse drums brings the reactor from approximately $6.40 subcritical to $1.60 subcritical.

The fine control drums are driven inward simultaneously by the actuators upon receipt of the controller power signal. Drum movement is achieved by an intermittent or stepping motion. A stepping motor-type actuator was chosen because it could more reliably withstand the severe environment of high temperature, vacuum, and nuclear radiation. The step size and stepping rate have been selected to give an average drum insertion rate of approximately 0.2° rotation per min.

4. Heat Shield Temperature Switch

During the startup sequence the heat shield must be ejected to allow for power heat rejection to space. The heat shield temperature switches initiate heat shield ejection when the reactor outlet temperature reaches the predetermined

value of approximately 275°F. The switches are located at the pump outlet and are connected in parallel for increased reliability.

Operation of the control system is extremely simple. After the startup command has been given, the signal obtained from the temperature sensor switch indicates that the reactor outlet temperature is below the set point or reference temperature. Therefore, the actuators drive the fine control drums inward, thus inserting reactivity and increasing reactor power and temperature. When the reactor outlet temperature rises above the reference temperature, the error signal is removed and drum rotation halted. If the outlet temperature of the reactor should fall below the reference temperature, the drums would again be rotated inward, thus inserting reactivity. Control action continues to maintain the reactor outlet temperature above the reference temperature until the controller off command is received.

The following is a description of the startup sequence (see Table 3).

TABLE 3

STARTUP TIME SEQUENCE

Item	Time
1. Expansion compensators released	After vehicle second burn
2. NPU start commanded	< 15 hr after launch
3. Drum locking pins released	10 msec after start command
4. Control system activated	10 msec after start command
5. Heat shield ejection circuits enabled	10 msec after start command
6. Coarse control drums inserted	10 msec after start command
7. Control system starts fine control drum insertion	50 sec after start command
8. Reactor goes critical	6.0 hr after start command
9. Discernible heat	6.33 hr after start command
10. Heat shield ejected	6.39 hr after start command
11. Reactor at initial operation point	9.75 hr after start command
12. System stabilized	72 hr after start command
13. Control system commanded off	72 hr after start command
14. Malfunction and failure circuitry enabled	72 hr after start command

After the vehicle second burn, the expansion compensator locking pins are released by firing the expansion compensator squibs. This allows the coolant to expand as the system is brought up to temperature. Upon confirmation of a long-life orbit, the startup command is given. At this time, the system is subcritical at ambient source power level and coolant is circulating at a minimum rate of 4% of design flow. The startup command enables the controller and heat shield ejection circuit, and fires the squibs that release the drum locking pins. The two coarse control drums are snapped in, thereby reducing the amount of subcriticality. The fine control drums then start their rotation inward, and reactor power rises. As more reactivity is inserted, the reactor becomes critical. The reactor power continues to increase with a decreasing period as reactivity is inserted. The increase in reactor power and temperature is temporarily reversed after the reactor reaches the power level of sensible heat generation. This is due to the negative reactivity introduced by the temperature coefficients of the grids and fuel.

During this initial power rise the reactor outlet temperature reaches the heat shield ejection set point, thus firing the squibs which allow ejection of the heat shield.

After the initial power transient, there is a gradual rise in power with corresponding rises in system temperatures and flows. This process continues until the reactor outlet reference temperature is reached. At this time, the controller stops the reactivity insertion. A decrease in reactor outlet temperature below the reference temperature actuates the controller to again insert reactivity. The control is left on for 72 hr to stabilize the system at rated conditions by compensating for the reactivity losses due to the hydrogen redistribution and xenon poisoning transient.

E. MATHEMATICAL MODEL OF THE SYSTEM

The first step in meeting the analysis objectives stated in Section IV-C was to mathematically describe the system and its environment. The second step was to obtain a solution of the resultant set of simultaneous equations. The balance of this section describes the methods employed in development of the mathematical model and a summary of the system components simulated.

The problem of mathematically representing the system can be divided into three major areas as follows:

1) Description of the temperature variation with respect to time throughout the NPU

2) Description of the nuclear behavior of the reactor; i.e., time variations of power and reactivity

3) Description of coolant flow with respect to time.

In addition to the above, the operation of the control system and the environment also must be represented.

The method of mathematically representing temperature variations throughout the NPU is the same as described in the prestartup analysis section. That is, the system components are divided into a series of lumps or nodes which are assumed to be of uniform temperature throughout. An energy balance is then performed on each of the nodes. The energy into and out of each node is determined by the appropriate heat transfer means. The difference between the energy flowing into the node and that flowing out is the stored energy, which is proportional to the temperature rate of change of the node. Thus, the energy balance takes the form of an ordinary differential equation in node temperatures with respect to time. These equations may be nonlinear, depending on the heat transfer mechanism and dependence of physical properties on temperature and other system variables.

The nuclear behavior of the reactor is simulated by a six delayed-neutron group model. The neutron kinetic equations take the form of seven differential equations. These equations are in normalized form with respect to initial conditions. The reactor forcing function, and for that matter the forcing function of the system, takes the form of reactivity introduced by motion of the fine control drum. When the total reactivity is zero, the reactor is critical and the number of fissions taking place during each neutron generation is constant. Thus, the power level of the reactor remains constant. An increase or decrease in the reactor power level is caused by a respective increase or decrease in the total reactivity from critical. The total reactivity is obtained by summing the reactivity feedback due to the temperature changes of the grid plate and fuel with the reactivity introduced by the control drums.

The coolant is caused to flow by means of an integral thermoelectric d-c conduction-type pump. The pump and the coolant flow are simulated in two parts. The first part consists of describing the pump heat transfer by means of nodal

energy balances, as described previously. The resultant equations relate the temperature difference across the thermoelectric material caused by the flow of heat from the hot coolant to the pump radiator. Some of the heat which leaves the hot coolant is not rejected to space but is converted to electrical energy (voltage and current) by means of Seebeck effect of the thermoelectric material. The electrical energy is, in turn, converted to mechanical energy by the pump. The mathematical representation of the flow induced by the pump is accomplished by performing a force balance at the pump throat. Electrical current through the coolant at the pump throat in the presence of a magnetic field produces a force tending to accelerate the coolant. This force is opposed by the hydraulic friction forces of the system and pump. In addition to the friction forces, the inertia force of the coolant mass must be overcome. Equating these forces results in a first-order nonlinear differential equation with flowrate as the dependent variable and temperature difference across the thermoelectric material as the forcing function.

Figure 25 is a block diagram of the system components simulated in the startup analysis. Also included in the simulation are solar heating for sun-shade transient and constant sun-constant shade orbits, as well as automatic heat-shield ejection.

The reactor heat transfer model consists of three fuel and coolant temperature nodes, as well as upper and lower grid and manifold nodes.

The pump model consists of seven temperature nodes and the differential equation describing the pump behavior. The hydraulic characteristics of the system, such as pressure drop and inertia of the coolant, are also included.

The control system simulation includes the temperature sensor switch, actuators (stepping motors), controller (power pulse generating circuits), and the fine and coarse control drums.

The transport delay of the lines to and from the reactor, as well as the upper and lower converter manifolds, are represented. Finally, a 24-temperature node model is used to simulate the converter-radiator and ejectable heat shield.

A total of 50 temperature nodes is used to represent the heat transfer of the system. (See Figure 26 for temperature node diagram.) One-hundred and nine equations (60 differential) are required to describe the dynamic behavior of the system, the basic equations of which are presented in Appendix B.

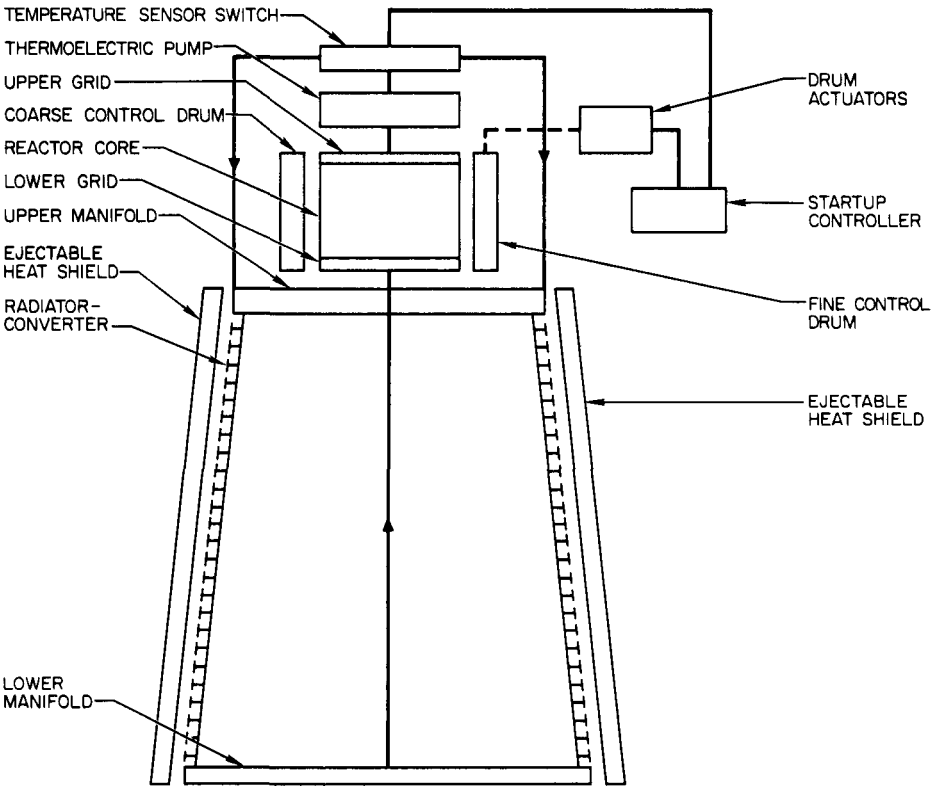

4-13-64 7561-01236

Figure 25. Simulated System Components

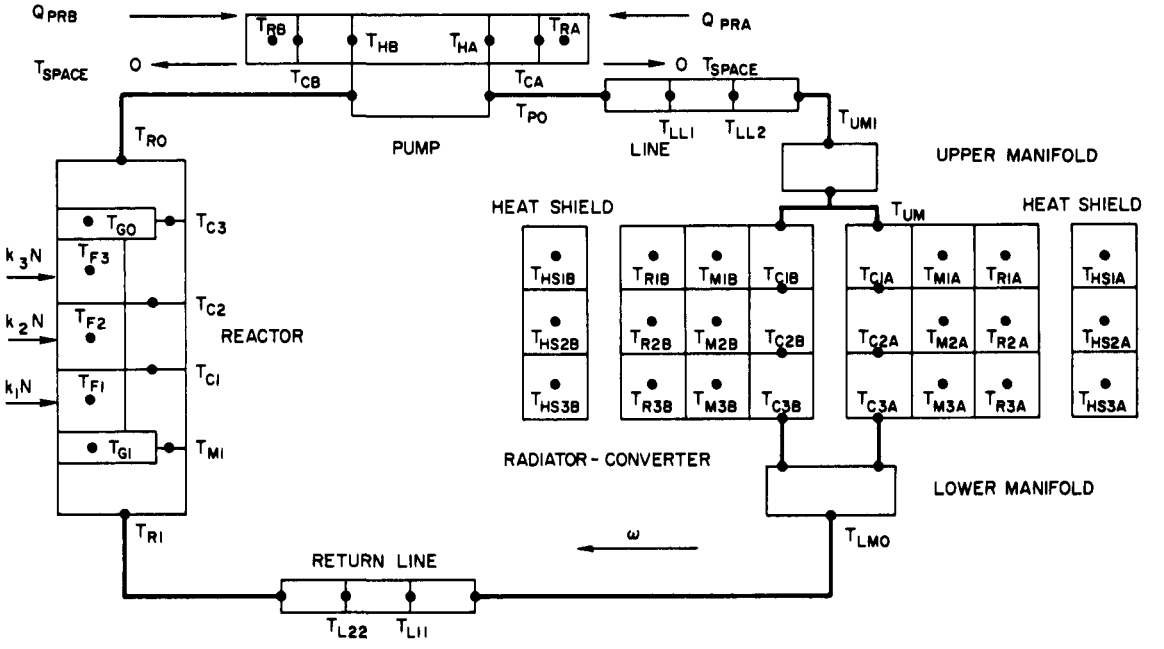

4-13-64 7561-01237

Figure 26. SNAP 10A Temperature Node Diagram

The solution of these equations is obtained in two parts. The first part consists of the use of the modified Airek III digital code to determine the behavior of the system from source power level to sensible heat, which is assumed to be 100 w. Only the reactor kinetics are considered in this part of the program, since the reactivity feedback through the reactivity temperature coefficients is essentially nonexistent until sensible heat generation.

The digital results provide the reactor kinetics initial condition data at sensible heat. The initial temperature conditions throughout the system at sensible heat are obtained from the results of the prestartup analysis.

The second part, solution of the system equations from sensible heat to steady-state operation, is accomplished by analog computer. Approximately 300 amplifiers and 4 consoles are required.

F. RESULTS

The behavior of the NPU from the time of the startup command to the start of sensible heat generation is obtained from the results of the modified Airek III digital code. The reactor power level and the delayed neutron group histories are presented in Figure 27. The results of Figure 27 are for a source power level of 10^{-11} kw, which corresponds to a source strength due to spontaneous fission. The drum insertion rate is taken at the nominal rate of 1/2° of inward rotation every 150 sec.

Six hours after the startup command is given, the reactivity insertion overcomes the shutdown reactivity and the reactor becomes critical. At this time, the reactor power level is approximately 40×10^{-11} kw, and the actuators have taken 144 1/2° steps rotating the fine control drums 72° inward. Although the reactor power generated increases forty-fold from the time the two coarse drums are snapped in to criticality, the additional energy generated is not sufficient to change the reactor temperatures. Therefore, the coolant flow and temperatures throughout the NPU are still determined by the passive environment of the prestartup phase.

As seen from Figure 27, the reactor power level continues to increase from the power level at criticality with an ever decreasing period. The reactor reaches the power level of sensible heat generation (100 watts thermal) approximately 19.4 min after criticality occurs. During this time, seven additional

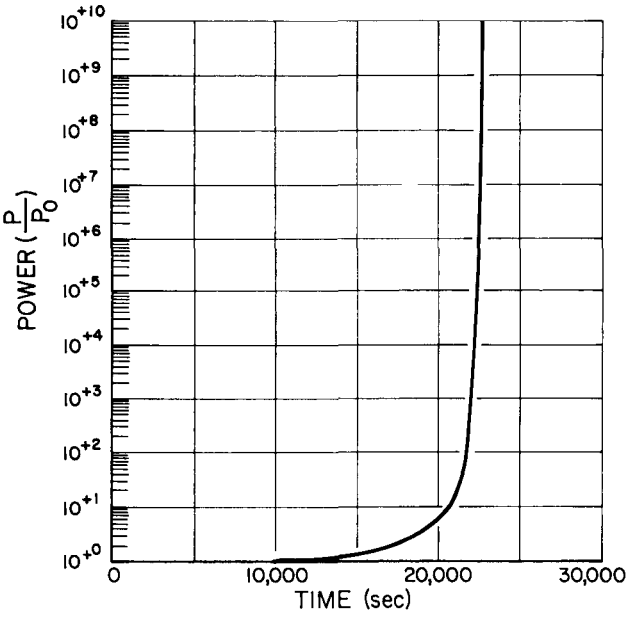

4-10-64 7561-01238a

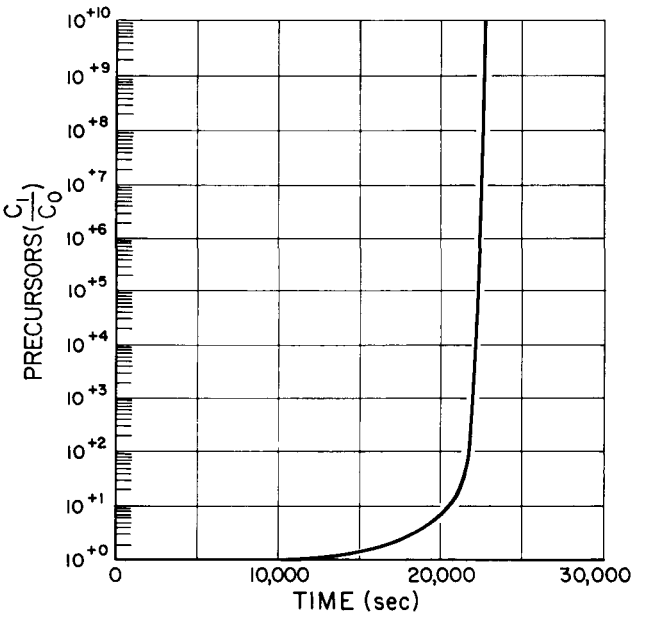

4-10-64 7561-01238b

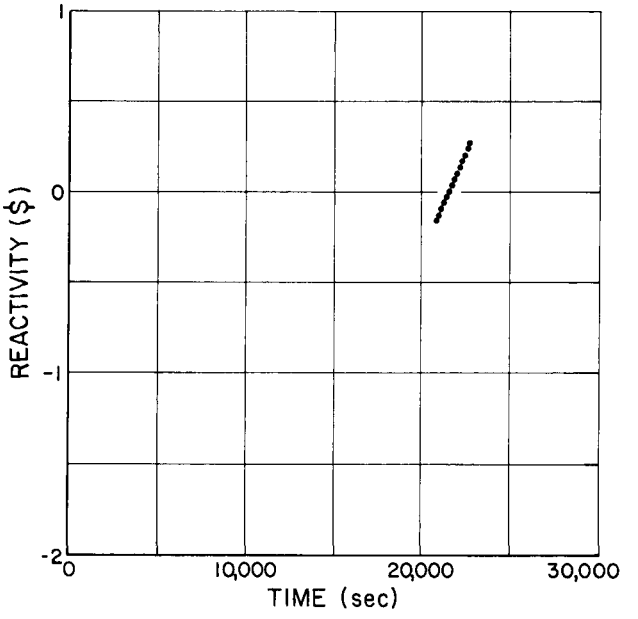

4-10-64 7561-01238c

Figure 27. Reactor Power Level and Delayed Neutron Group Histories

control drum steps are taken, placing the drums 75.5° rotated inward. The reactor power is now increasing on a 26.4 sec period which corresponds to an excess reactivity of 24.2¢.

A total of nine additional cases of various stepping rates and initial reactor temperatures are run using the modified Airek III code. The results of these runs are used to provide initial conditions for the reactor kinetics portion of the subsequent analog computer study covering sensible heat to full-power operation.

Figures 28 and 29 have been prepared from run results. Figure 28 shows the relationship of excess reactivity at sensible heat for various control-system stepping rates and source-strength power levels. The discontinuous relationship between excess reactivity and source-strength power level is due to the manner in which reactivity is inserted. That is, reactivity is inserted in steps causing a staircase-type increase in reactivity, as opposed to a continuous ramp increase. It is of interest to note that a source strength variation of two decades can result in no change of excess reactivity and, therefore, period at sensible heat. The effect of source strength and stepping rate on the time from criticality to sensible heat is presented in Figure 29.

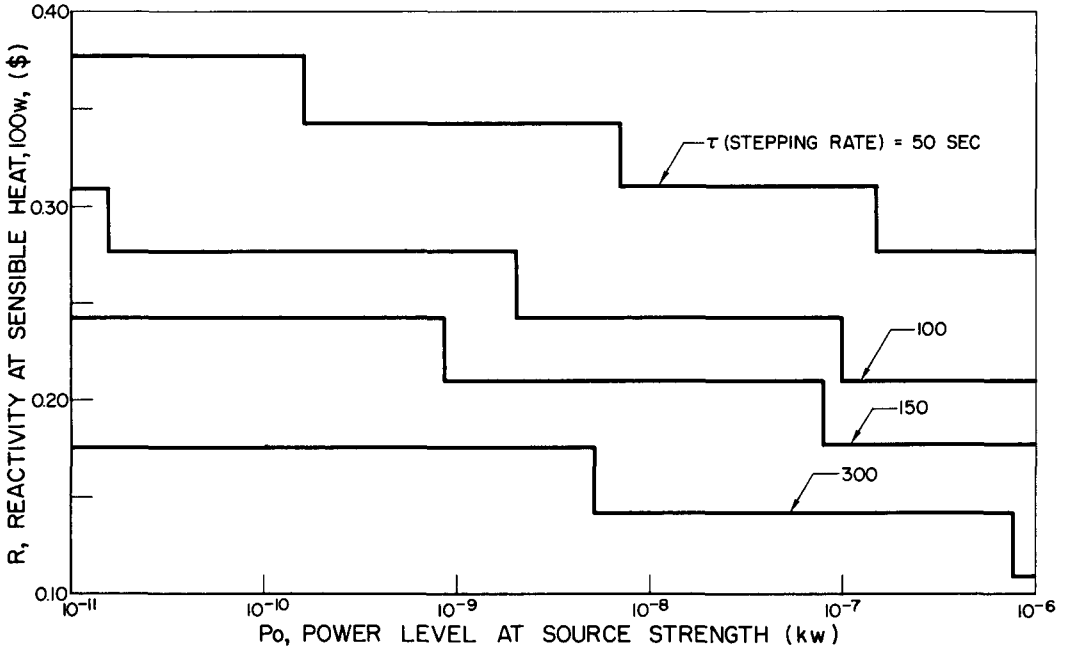

Figure 28. Excess Reactivity at Sensible Heat

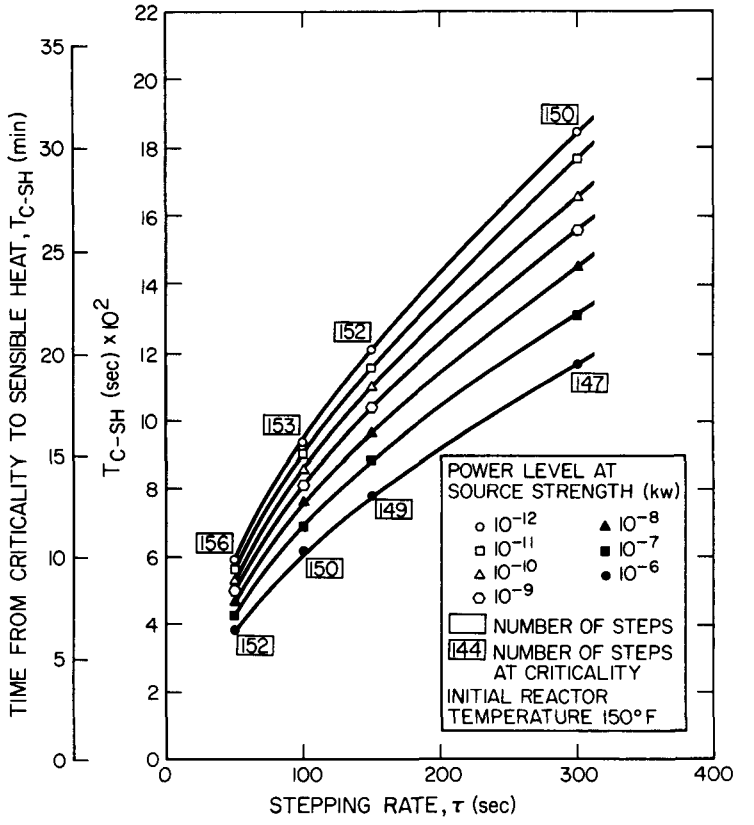

4-13-64 7561-01240

Figure 29. Time From Criticality to Sensible Heat

The histories of the system parameters from sensible heat generation to full power are shown in Figure 30. The startup transient illustrated is felt to be representative of a typical startup in space, and it corresponds to the fixed system parameters and nominal value of varied parameters summarized in Tables 4 and 5, respectively.

Referring to Figure 30, the analog computer recording continues from the point in time where the digital code leaves off. That is, the reactor power level increasing on 26.4 sec period. As the power level continues increasing from the sensible heat generation level, the fuel and coolant temperatures of the reactor begin to rise. However, because temperatures of fuel and coolant lag the power, the reactivity feedback caused by reactor temperature change does not reverse the power transient until 155 sec after sensible heat occurs. At this time, the reactor reaches a peak power of 56 kw. The reactor outlet temperature corresponding to this peak power spike is 420°F and occurs 70 sec after the power

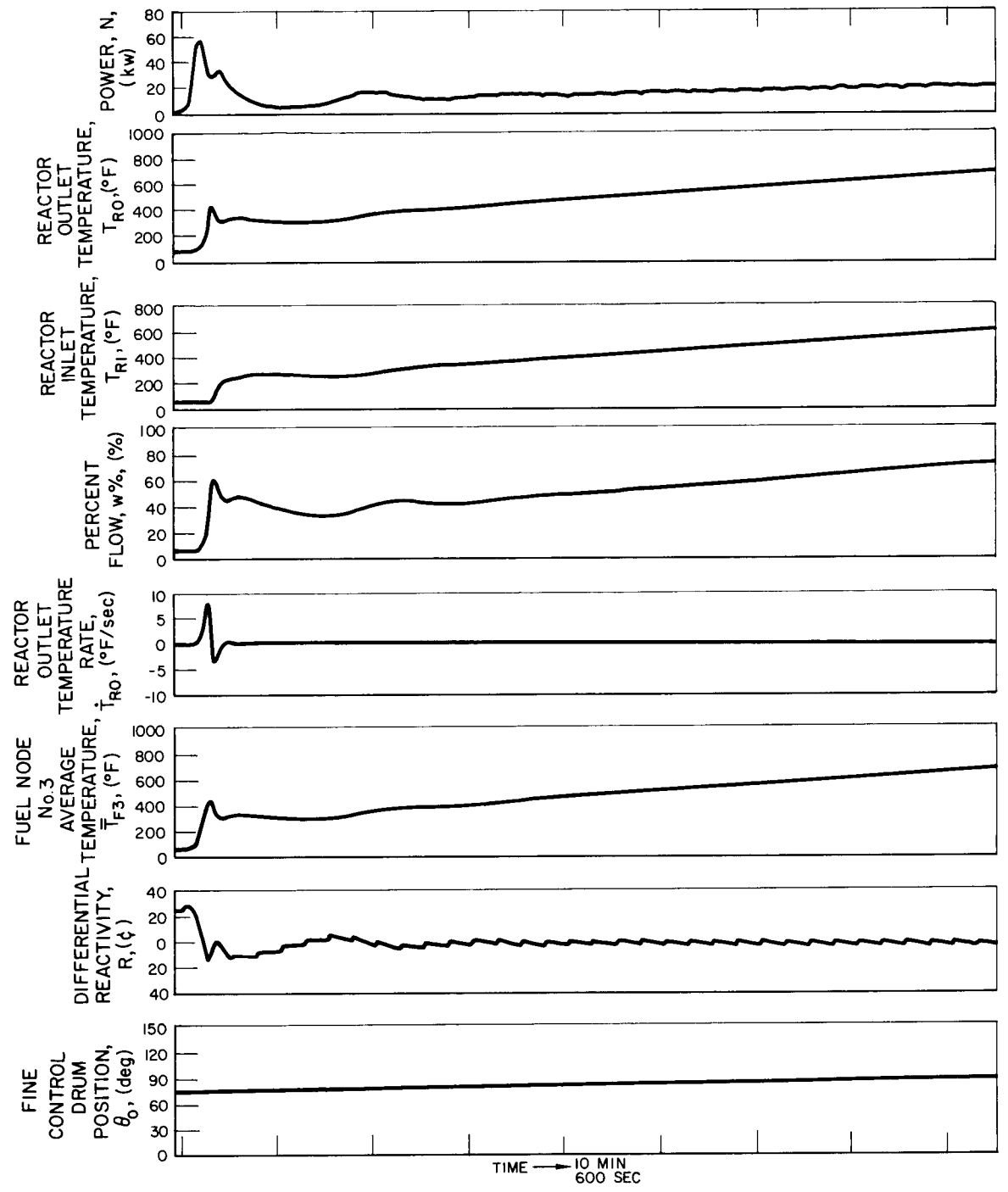

4-13-64

7561-01243

Figure 30. Startup Transients, Nominal Case

TABLE 4

FIXED SYSTEM PARAMETERS

Reactor	
R_O (shutdown reactivity)	-$5.60
C_{PF} (specific heat of fuel)	$0.09462 + \frac{0.04947}{1000} T_F$ $\frac{kw\text{-}sec}{lb/°F}$
R_{CD} (drum worth)	See Figure 24
Control system	
θ_D (drum insertion)	1/2° step
τ_D (controller delay)	50 sec
τ_{TS} (temperature sensor switch time constant)	58 sec
T_{SP} (nominal temperature set point)	1010°F ± 10°F
Hydraulic	
ΔP_{SYS} (system pressure drop)	1.1 psi at 100% flow (see Figure 31)
I_{SYS} (system inertia)	0.421 $sec^2/in.^2$
τ_{Loop} (loop cycle time)	17 sec (at 1000°F and 100%-$\dot{W}$)
Other startup parameters	
$\dot{W}_O$% (initial NaK flow)	4%
T_{HS} (heat shield ejection temperature)	275°F at reactor outlet

TABLE 5

VARIED PARAMETERS

Parameter	Nominal	Variation
$\bar{U}A$, Reactor heat transfer coefficient	See Figure 32	See Figure 32
PO, Power at source strength	10^{-11} kw	$10^{-11} \rightarrow 10^{-9}$ kw
Reactivity coefficients		
αGO – upper grid	-0.05¢/°F	±0.02¢/°F
αG1 – lower grid	-0.05¢/°F	±0.02¢/°F
αF – fuel	$-(0.074 + \frac{0.066}{1000}\bar{T}_F)$¢/°F	±0.03¢/°F
τ_{SR}, Controller stepping rate	150 sec	$^{+30}_{-20}$ sec
Pump performance at design conditions	100%	100% → 60%

peak. The maximum instantaneous reactor outlet temperature rate is 9.5°F/sec, occurring 45 sec after peak power. The reactor inlet temperature remains constant at its initial value until 240 sec after peak power. Therefore, the lower grid plate has no effect on the initial power and temperature transient.

Approximately 215 sec after sensible heat generation during the initial reactor excursion, the reactor outlet temperature reaches 275°F. Thus, the heat shield is ejected. Examination of the recorded results indicates that ejection of the heat shield during startup has no perceptible effect on the system. This result confirms earlier studies which concluded that ejection of the heat shield would not cause excessive thermal stresses, shock, or any other adverse effects.

After the initial power excursion, the continued insertion of reactivity again causes the reactor to go critical. Therefore, the reactor power starts to increase once more. However, the reactor is on a relatively large period and the increase in power, system temperatures, and flow is slow. The rest of the startup transient is uneventful. As the drums are stepped in at a constant rate, the system slowly rises to initial operating conditions corresponding to a reactor outlet temperature 1010°F. It is noted that the rate at which reactor outlet temperature increases becomes less as the temperature approaches its full power value. This is due to the shape of the drum worth curve (Figure 24). That is, although the drums are inserted at a constant rate, the worth of each drum step decreases as the drums approach the full-in position.

The total time elapsed from the startup command to initial full power is 9.75 hr, of which 3 hr and 25 min are required to go from sensible heat to full power.

Figure 31 illustrates the behavior of the reactor outlet temperature at end of the startup transient and the beginning of the stabilization period of control. Prior to the temperature sensor switch closing (t = 0), the reactor outlet, inlet, and sensor switch temperatures are increasing at a rate of 3°F/min. It is seen that the sensor switch temperature is lagging the reactor outlet temperature by the switch thermal time constant τ. Therefore, when the sensor temperature reaches the set-point temperature, the reactor outlet temperature will exceed

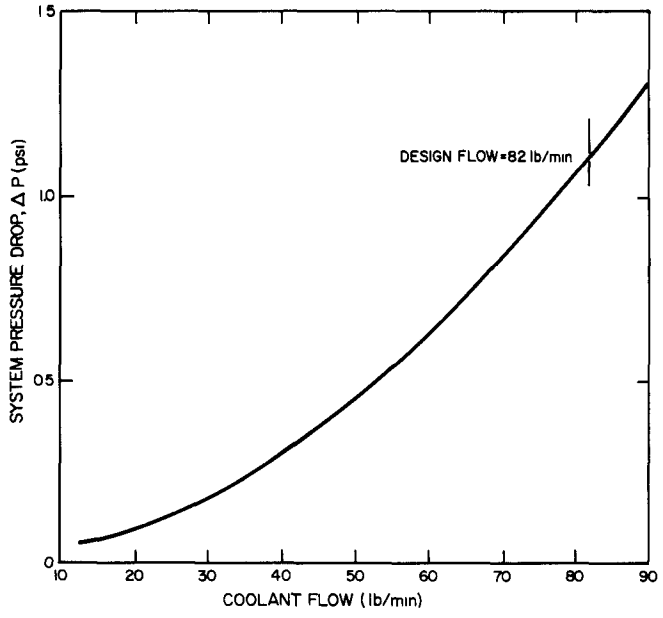

Figure 31. ΔP System Pressure Drop

4-13-64 7561-01241

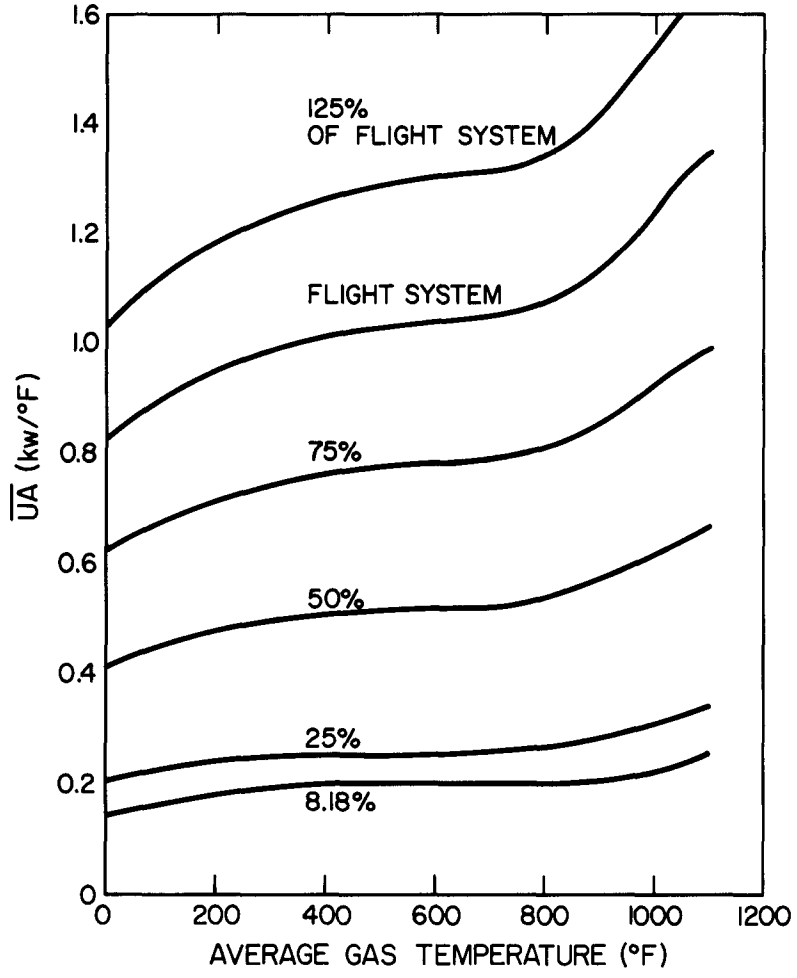

Figure 32. Reactor Heat-Transfer Coefficient

4-10-64 7561-01242

the set-point temperature by the amount equal to the product of the switch time constant, τ, and the reactor outlet temperature rate of change a. For this example, τa = 1 min x 3°F/min = 3°F.

The set point of the temperature sensor switch is adjusted to the nominal value of 1010°F. However, a switch closure in the range of 1000 to 1020°F for an increasing reactor temperature is acceptable. If it is assumed that the sensor is activated at its upper temperature set-point limit of 1020°F, the corresponding coolant temperature at the reactor outlet will be 1023°F.

When the temperature sensor switch closes, reactivity insertion ceases. However, the reactor outlet temperature continues to increase at the same rate as before, even though no more reactivity is being inserted. This effect is due to the thermal and nuclear time constants of the system; that is, the system has not as yet reached steady-state. The results of this study show that the reactor outlet temperature will continue to increase for approximately 2.5 min after the last reactivity step. It is assumed (although this is not the most probable case) that the reactivity is stepped just prior to the sensor switch closing. Therefore, the reactor outlet temperature will continue to increase for another 2.5 min, reaching a maximum temperature of 1030.5°F (at t_1).

At the time the sensor switch closes, the reactor is generating 44 kw of power. Approximately 2.5 of the 44 kw are being absorbed in the form of heat storage energy by large, thermal time-constant system components which have not as yet reached steady-state. When the system reaches steady-state, the 2.5 kw of energy that are going into storage must be accounted for by either an increase in the power being dissipated to space or a decrease in the reactor power requirements. Because of the large amount of negative reactivity feedback, the reactor tries to maintain a constant average temperature. Therefore, the reactor power level decreases to 41.5 kw to account for the decrease of energy going into storage. As seen from Figure 33, the reactor outlet temperature, as well as power level, decreases. Twenty-five minutes after the sensor switch first closes, the reactor outlet temperature is 1020°F and in another 25 min the temperature temporarily stabilizes at 1017°F. As the reactivity losses due to hydrogen redistribution and xenon poisoning gradually build up, the reactor outlet

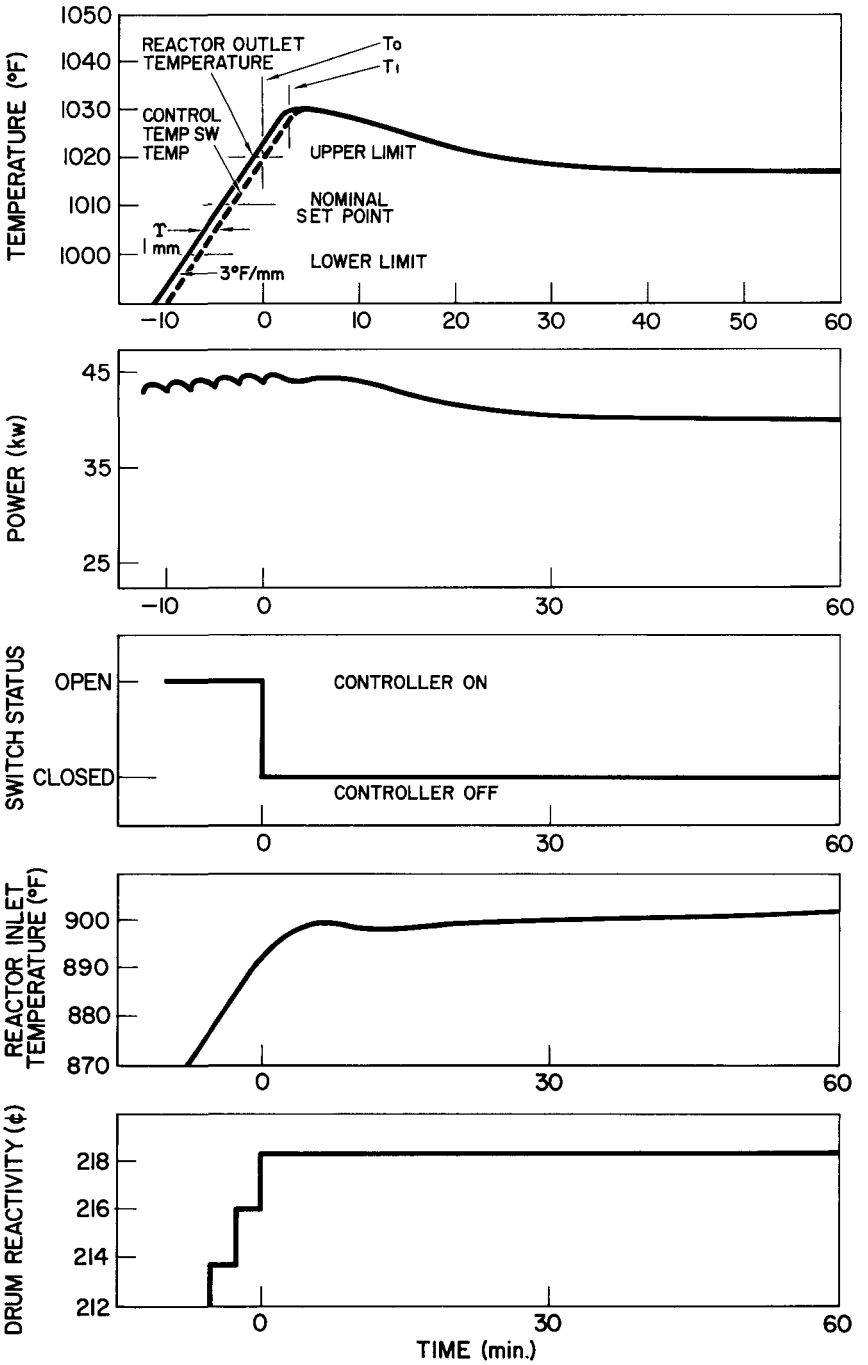

FIGURE 33 – SYSTEM BEHAVIOR AT THE START OF THE STABILIZATION PERIOD

4-1-64 7561-01244

Figure 33. System Behavior at Start of Stabilization Period

temperature will start to fall until the temperature is below the set point and reactivity is again inserted.

The effect of variations of critical system parameters on the startup transients is presented in the form of a series of plots, Figures 34 to 39. These plots were prepared from the recordings of 39 computer runs, and they illustrate the effect of parameter variations on peak power and reactor outlet temperature, as well as maximum rate of change of reactor outlet temperature. The parameters varied and the range of variation are summarized in Table 5. It is felt that the range of parameter variations studied is large enough to more than adequately cover any parameter value uncertainties.

Two factors have the most pronounced effect of the startup transient. They are excess reactivity at sensible heat and the reactivity temperature coefficient of the fuel. The excess reactivity occurring at sensible heat determines the period on which reactor power is increasing. The larger the excess reactivity, the faster the reactor power rise will be and, therefore, larger peak transient values will occur before the negative reactivity feedback can take effect.

The two parameters varied, which affect the excess reactivity at sensible heat, are stepping rate and power level at source strength (Figures 34 and 35). The relationship of these two parameters to excess reactivity is shown in Figure 28.

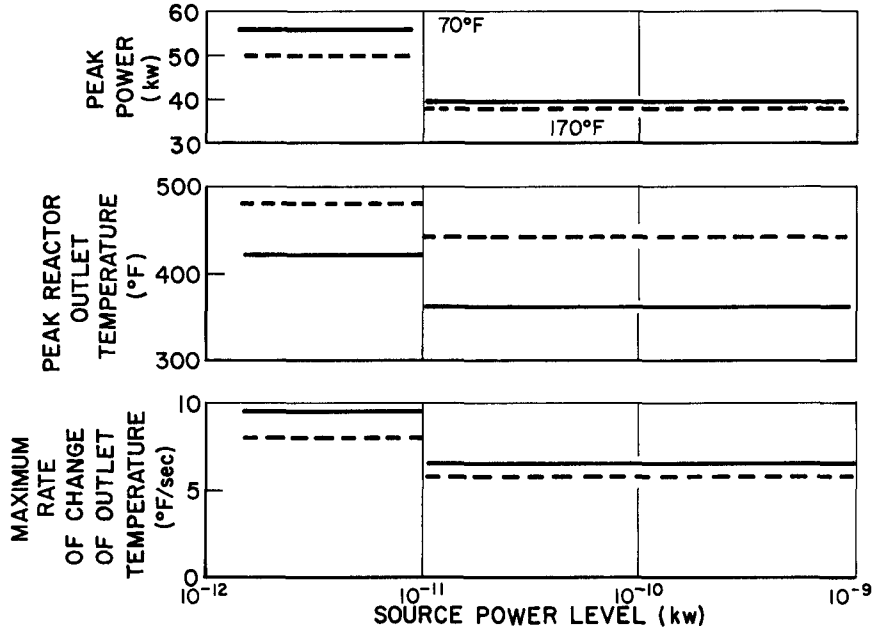

4-10-64 7561-01245

Figure 34. Effect of Source Power Level

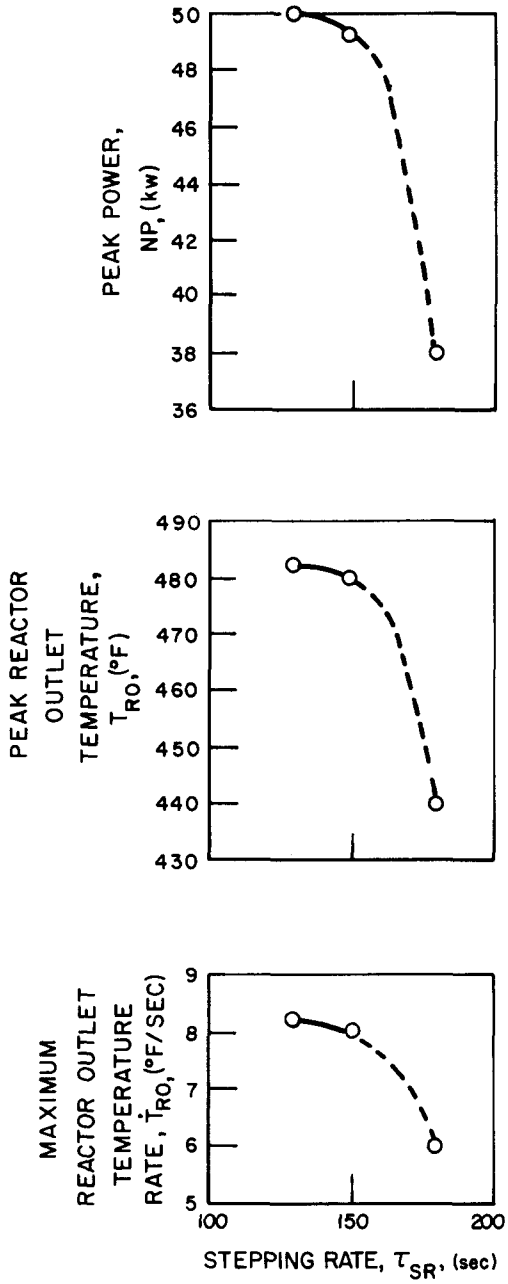

4-10-64 7561-01246

Figure 35. Effect of Stepping Rate

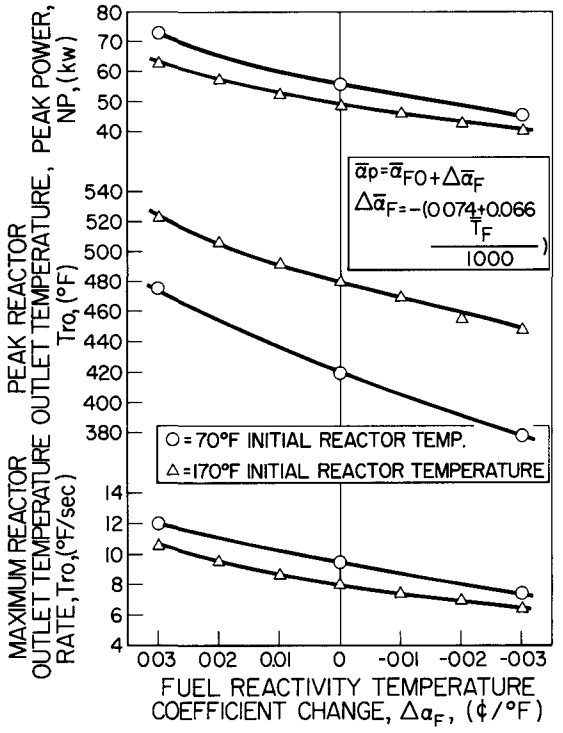

4-8-64 7561-01247

Figure 36. Effect of Fuel Reactivity Temperature Coefficient Changes

Figure 37. Effect of Reactor Heat Transfer Coefficient

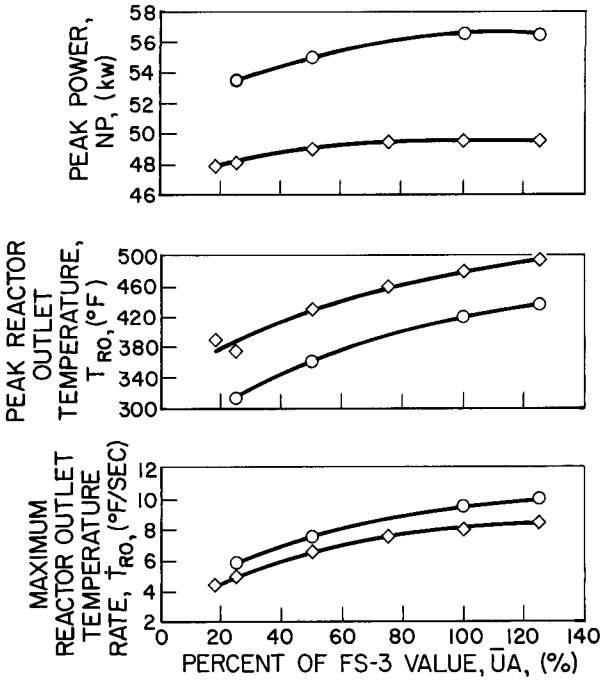

4-9-64 7561-01248

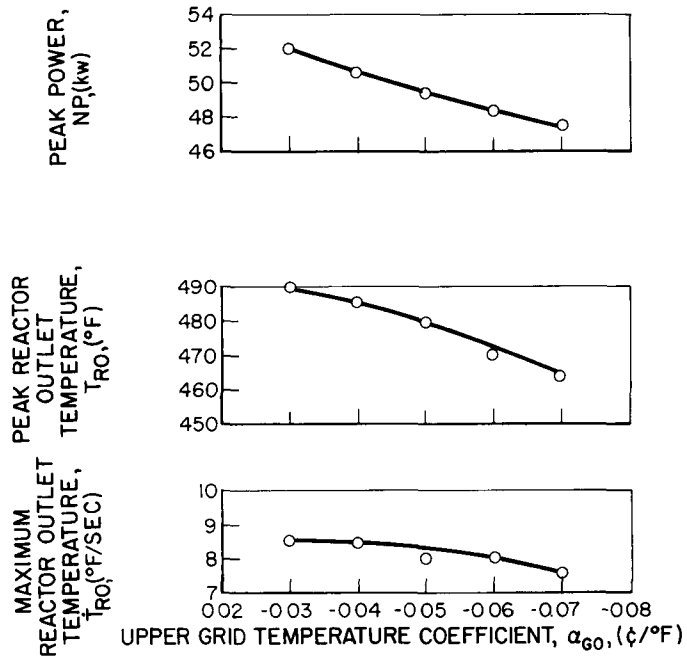

Figure 38. Effect of Grid Temperature Coefficient

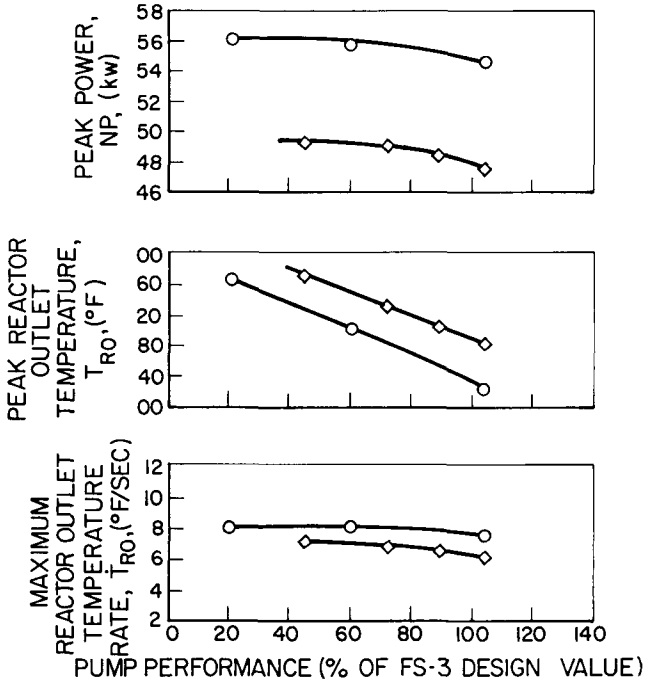

Figure 39. Effect of Pump Performance

The negative reactivity feedback through the fuel and upper and lower grid plates causes the reversal of the initial power excursion. Of these three feedback paths, the fuel reactivity feedback is the most important. It is obvious that the fuel located in the reactor core is the first to respond to the energy being released by the increasing nuclear fissions. Therefore, variations in the fuel reactivity temperature coefficient have a significant effect on the transient behavior of the system (Figure 36).

The lower grid-plate coefficient has no effect on the initial startup transient. This fact is due to the loop cycle time and thermal response of the system. That is, the lower grid-plate temperature experiences no change until after the initial power excursion occurs.

The effect of variations of the upper grid-plate reactivity coefficient is shown in Figure 38. As would be expected, variation of the upper grid-plate coefficient has less of an effect on the initial transient than the fuel coefficient. This is due to the larger increment of time required by the upper grid temperature to respond to a power change than that required by the fuel temperature.

The effect of variations of the fuel-coolant heat transfer coefficient ($\overline{UA}$) is shown in Figure 37. Peak power is virtually insensitive to large variations of the heat transfer coefficient. Peak reactor outlet temperature decreases with decreasing $\overline{UA}$, as expected.

Finally, variation of pump performance on the startup transient is shown in Figure 39. The only significant effect pump performance has on the initial power excursion is that of reactor outlet temperature. The peak reactor outlet increases in a linear manner with decreasing pump performance.

Some of the key factors in the startup transient response are summarized in Table 6. Also included in Table 6 are the values of these factors for the nominal design conditions and for the range corresponding to parameter variations. In general, the startup transient is less severe than previous studies indicated.

The results of the analysis just described are used as inputs to subsequence analyses and tests. The purpose of these studies and tests is to determine if the resultant startup transients predicted would impose any thermal shocks, stresses, or temperatures that would jeopardize system integrity. Thermal stress analyses of the reactor core, pump, and radiator converter, as well as many other

TABLE 6

SUMMARY OF ANALYSIS RESULTS

Variable	Nominal Value	Range
Peak power (initial power excursion)	56.5 kw	34.4 → 73 kw
Peak reactor outlet temperature (initial power excursion)	420°F	314 → 523°F
Peak flowrate (initial power excursion)	62%	45 → 69.1%
Maximum instantaneous rate of change of reactor outlet temperature	9.5°F/sec	4.5 → 12°F/sec
Time from startup command to criticality	6.0 hr	5.2 → 7.2 hr
Time from criticality to initial operating conditions	3.75 hr	3.25 → 4.50 hr
Maximum power overshoot (start of stabilization period)	44 kw	43 → 44 kw
Maximum reactor outlet temperature overshoot (start of stabilization period)	1030°F	1003 → 1030°F
Initial stabilized power level	38 kw	– –
Initial stabilized reactor outlet temperature	1017°F	1000 → 1017°F

system components, indicate no adverse effect due to the startup transient range predicted. In addition to these stress analyses, system components have successfully been qualified by thermal tests established by the predicted startup transient. Finally, a detailed nonnuclear system startup test was performed (FSM-1). The nonnuclear system is a duplicate of the flight system, except that the nuclear core is replaced by an electrical heater. The FSM-1 system was simulated, and the electrical power program required to force the core-heater outlet temperature to duplicate the predicted reactor outlet temperature was determined. As a result, the FSM-1 system, exclusive of the reactor, experienced the same startup transient as that predicted for the flight system. The results of the FSM-1 test indicate that no component or system failures are induced by thermal stress or shocks of the startup transient.

G. COMPARISON OF TEST RESULTS

The results of any analysis are no better than the mathematical model used to represent the system studied and the means of solution of the mathematical representation. In an effort to determine the validity of the startup analysis model and, therefore, the predicted results, a comparison was made between

the model results and the results of two ground tests. The nuclear reactor portion of the model was compared with results of tests on the SNAP 2 Developmental Reactor (S2DR). The S2DR test conditions were simulated as close as practical on the computer, and the results compared to the S2DR test results. The S2DR test results indicate a peak power of 46 kw for a 28¢ ramp insertion of reactivity at 2.1¢/sec. The computer results show a peak power of 53 kw for a 28¢ step insertion of reactivity. In light of differences between the S2DR test system and the flight system simulated, the results show very good correlation.

The nonnuclear portions of the model were compared with the results of the FSM-1 system test. The comparison of reactor outlet and inlet temperatures, as well as flow, is presented in Figure 40. The solid lines represent the system variable histories as predicted by the analysis. The circled points represent the FSM-1 test data obtained from oscillographic recordings. Once again, the analytical and test results show good correlation.

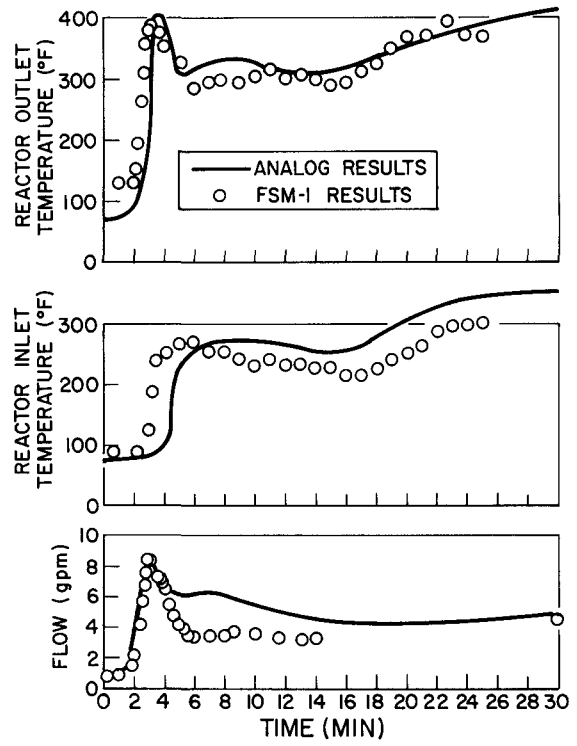

4-9-64 7561-01292

Figure 40. FSM-1 Startup Transient Results

V. CONCLUSION

Results of the SNAP 10A Prestartup, Startup, and Control analyses, and subsequent analyses based on the results, demonstrate that the following requirements are met by the present system.

a) The prestartup thermal conditions, following an extended period in the space environment, will be such that the system will start up in a normal manner.

b) The Startup and Control System will bring the NPU from a subcritical low-temperature state to criticality, sensible heat, initial operating conditions, and finally to stabilized operating conditions remotely and automatically while in orbit.

c) The NPU will be brought to rated operating conditions in such a manner that the resultant startup transients will not impose thermal shocks, stresses, or temperatures that would jeopardize system integrity.

d) The NPU will operate in a stable manner, thus minimizing thermal cycling of the system and control component wear.

BLANK

APPENDIX I

A. EFFECTIVE SPACE TEMPERATURES

For a given node j on the outside of the NPU, the net heat entering per unit area from space is

$$\frac{q_{net}}{A_j} = Q_{ds} + Q_{rs} + Q_{te} - \sigma\epsilon_j T_j \ . \qquad \ldots(1)$$

This net heat is represented by an expression of the form

$$\frac{q_{net}}{A_j} = \epsilon_j\sigma \left(T_{eff}^4 - T_j^4\right) \qquad \ldots(2)$$

which provides the defining equation for T_{eff}

$$T_{eff} \equiv \left(\frac{Q_{ds} + Q_{rs} + Q_{te}}{\epsilon_j\sigma}\right)^{1/4} \ . \qquad \ldots(3)$$

The direct solar radiation is given by

$$Q_{ds} = \alpha_j f(\varphi) \sin\gamma\, q_s \qquad \ldots(4)$$

where

$$f(\varphi) = \begin{cases} \sin(\varphi + \delta), & 0 \le \varphi < \frac{\pi}{2} + \theta \\ 0, & \frac{\pi}{2} + \theta \le \varphi < 2\pi - \delta \\ \sin(\varphi + \delta), & 2\pi - \delta \le \varphi < 2\pi \end{cases}$$

and

$$\theta = \cos^{-1}\frac{R}{R + h}$$

The thermal earth radiation is given by

$$Q_{te} = \epsilon_j F_{se} \sigma T_e^4 \qquad \ldots(5)$$

where the satellite-to-earth view factor is based on a conical body above the earth, and is given by

$$F_{se} = \frac{2\left(\frac{\pi}{2} - \theta - \delta\right) - \sin\left(\frac{\pi}{2} - \theta - \delta\right)}{2\pi} .$$

The reflected solar radiation is given by

$$Q_{rs} = \alpha_j F_{se} q_s \overline{\cos \omega} \, r_{es} \qquad \ldots(6)$$

Since this input is small, an approximate analysis has been used to evaluate the mean cosine of the angle of incidence of the sun's rays on the earth. The key assumptions are as follows:

1) Azmuthal angle variations are neglected.

2) As the vehicle enters the shade, the value of $\overline{\cos \omega}$ drops linearly to zero.

As a result of these assumptions, three regions are delineated in the orbit, as follows:

1) Region A — All of the earth seen by a node on the NPU is sunlit.

2) Region B — A portion of the earth seen by a node on the NPU is shaded.

3) Region C — All of the earth seen by a node on the NPU is shaded.

Table 7 presents the values used to express $\overline{\cos \omega}$ in each of these regions.

For a circular orbit, the above expressions may be expressed in terms of time, τ, by the substitution

$$\varphi = \Omega \tau \qquad \ldots(7)$$

TABLE 7

$\overline{\text{Cos } \omega}$ VALUES

Range	Region	$\overline{\cos \omega}$
$0 \leq \varphi < \frac{\pi}{2}$	A	$\frac{1}{\theta}\left[\sin \varphi - \sin (\varphi - \theta)\right]$
$\frac{\pi}{2} \leq \varphi < \frac{\pi}{2} + \theta$	B	$\frac{\frac{\pi}{2} + \theta - \varphi}{\theta} (1 - \cos \theta)$
$\frac{\pi}{2} + \theta \leq \varphi < \frac{3\pi}{2}$	C	0
$\frac{3\pi}{2} \leq \varphi < \frac{3\pi}{2} + \theta$	B	$\frac{\varphi - \frac{3}{2}\pi}{\theta}(1 - \cos \theta)$
$\frac{3\pi}{2} + \theta \leq \varphi < 2\pi$	A	$\frac{1}{\theta}\left[\sin \varphi - \sin (\varphi - \theta)\right]$

For evaluation in the computer, the results of the above defining equations for T_{eff} were evaluated by an approximate expression which provided three regions; a sinusoidal region, a constant region, and a linear region which are taken on successively as the angle φ increases from zero to 2π.

The above expressions apply to the sun-shade transient orbit. It is important to note that in addition to the symmetry plane used to reduce the number of nodes, a plane of antisymmetry exists for the sun-shade transient orbit which is determined by the vehicle yaw-pitch axes. For nodes symmetrically located with respect to this plane, the following relation applies:

$$T_{eff}(\varphi) = T'_{eff}(2\pi - \varphi) .$$

For the constant sun-constant shade orbit, the effective space temperatures are independent of time. They have the same value as is taken on in the sun-shade equations when the vehicle is over the North Pole ($\varphi = \pi/2$).

B. PROGRAM EQUATIONS

Consider a three-dimensional system of heat transfer nodes in which there is conduction, radiation, and bulk transport or convection, as in Figure 41.

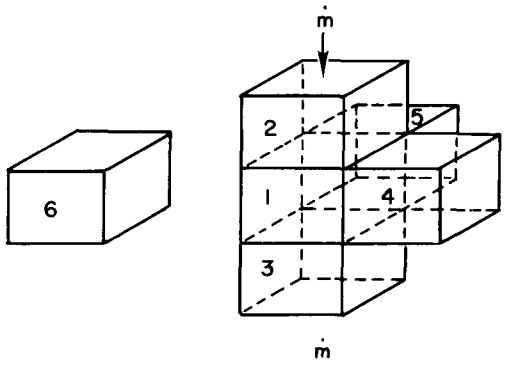

Figure 41. Three-Dimensional Heat-Transfer System

Assume that there is mass flow between nodes 2 and 1, and 1 and 3, which makes conduction between these nodes negligible; that there is radiation only from node 6; and that there is conduction only between nodes 1 and 4, and 1 and 5. The energy equation for an incompressible nonviscous fluid is

$$m_1 c \frac{DT_1}{D\tau} = Q \, . \qquad \ldots(8)$$

For one-dimensional flow,

$$\frac{DT_1}{D\tau} = \frac{\partial T_1}{\partial \tau} + \frac{\partial T_1}{\partial x} \frac{dx}{d\tau} = \frac{\partial T_1}{\partial \tau} + u_1 \frac{\partial T_1}{\partial x} \qquad \ldots(9)$$

where

$$u_1 = \frac{\dot{m}_1}{\rho A} \, . \qquad \ldots(10)$$

Substituting Equations 9 and 10 in Equation 8, and approximating the derivatives by their first-back differences,

$$T_{1,\Delta\theta} = T_1 + \frac{\dot{m}_1}{m_1}(T_2 - T_1)\,\Delta\tau + \frac{Q_1}{m_1 c}\,\Delta\tau \qquad \ldots(11)$$

is obtained after rearrangement.

Equation 11 gives the temperature of node 1 after some time increment, $\Delta\tau$, in terms of its initial temperature, the flowrate to the node, its heat capacity, and the heat transferred in from adjacent nodes. The heat transfer, Q_1, is due to conduction and radiation and may be expressed as

$$Q_1 = U_4(T_4 - T_1) + U_5(T_5 - T_1) + \sigma A_1 \mathcal{F}_{16}\left(T_6^4 - T_1^4\right). \qquad \ldots(12)$$

Equation 12 may be substituted in Equation 11 and the results generalized and expressed compactly as

$$T_{i,\Delta\theta} = T_i + \sum_j C_{ij}(T_j - T_i) + \sum_j R_{ij}\left(T_j^4 - T_i^4\right) \qquad \ldots(13)$$

where the radiation coefficients are given by

$$R_{ij} = \frac{\sigma A_i \mathcal{F}_{ij} \Delta\tau}{m_i c} \qquad \ldots(14)$$

and the conduction and bulk transfer coefficients are given by

$$C_{ij} = \frac{U_{ij}\Delta\tau}{m_i c} \quad \text{or} \quad \frac{\dot{m}_i \Delta\tau}{m_i} \quad . \qquad \ldots(15)$$

Equation 13 is in a form which may be readily programmed for a digital computer.

C. EQUATIONS FOR PARAMETRIC ANALYSIS

To evaluate the effect on minimum NaK temperature of changes in α_S, ϵ_i, ϵ_o, an equivalent change in the effective space temperature is computed. This is done on the basis of average hot- and cold-side temperatures. The objective of the analysis is to find a change in effective space temperature which would

produce the same change in heat leaving the radiator converter as the changes in α_S, ϵ_i, and ϵ_o, would produce. Assuming the heat shield is approximately in equilibrium, the net heat leaving the radiator per unit area is

$$q_R = \frac{\epsilon_i}{\epsilon_i + \epsilon_o}\left(\sigma\epsilon_o T_{RH}^4 - K_1\alpha_S - K_2\epsilon_o\right). \qquad \ldots(16)$$

The constants K_1 and K_2 are to be obtained by appropriately averaging the solar and thermal earth inputs. This heat may also be exprssed in terms of the effective space temperature as

$$q_R = \sigma \frac{\epsilon_i\epsilon_o}{\epsilon_i + \epsilon_o}\left(T_{RH}^4 - T_{eff}^4\right) . \qquad \ldots(17)$$

The desired change in effective space temperature may then be found from the expression

$$\frac{\partial qR\rightarrow}{\partial T_{eff}}\Delta T_{eff} = \frac{\partial qR\rightarrow}{\partial \epsilon_i}\Delta\epsilon_i + \frac{\partial qR\rightarrow}{\partial \epsilon_o}\Delta\epsilon_o + \frac{\partial qR\rightarrow}{\partial \alpha_S}\Delta\alpha_S \qquad \ldots(18)$$

where the partial derivatives are to be obtained from Equations 16 and 17, and evaluated at conditions occurring during the first orbit.

To determine the effect on maximum heat-shield temperature of changes in α_S, ϵ_i, and ϵ_o, a heat balance is made on the heat shield to provide the following expression for average heat shield temperature:

$$T_{HH}^4 = \frac{\sigma\epsilon_i T_{RH}^4 + K_1\alpha_S + K_2\epsilon_o}{\sigma(\epsilon_i + \epsilon_o)} . \qquad \ldots(19)$$

The radiator temperature may be eliminated by assuming the overall system to be in equilibrium, and taking the radiator temperature as being equal to the core outlet temperature. If this is done, we obtain

$$T_{HH}^4 \cong \frac{K_2}{\sigma} + \frac{K_1 \alpha_5}{\sigma(\epsilon_o + \epsilon_i)} \left[1 + \frac{\epsilon_i}{2\epsilon_o} \right] . \qquad \ldots(20)$$

The expected change in heat shield temperature due to a change in system thermal properties may be estimated from this equation by evaluating it at the base case and at values corresponding to the worst expected shift in values.

D. NOMENCLATURE

Symbol	Description	Dimensions
A	Area	ft^2
c	Heat capacity	Btu/lb-°F
C_{ij}	Heat transfer constant	Dimensionless
$F, \mathcal{F}$	Geometrical or net interchange factor	Dimensionless
h	Orbital altitude	mi
K	Constant of proportionality	Btu/hr
m	Mass	lb
$\dot{m}$	Mass rate	lb/hr
q, Q	Heat flowrate	Btu/hr
r	Reflectivity	Dimensionless
R	Radius of earth	mi
R_{ij}	Heat transfer constant	$°R^{-3}$
T	Temperature	°R
U	Conductance	Btu/hr-°F
u	Velocity	ft/hr
x	Length	ft
Greek Letters		
α	Solar absorptivity	Dimensionless
γ	Angular location of node on NPU	radians
δ	Half apex angle of cone	radians
ϵ	Thermal emissivity	-
θ	Angle defined by local vertical and horizon	-
ρ	Density	lb/ft^3
σ	Stefan-Boltzman constant	0.171×10^{-8} $Btu/ft^2\text{-hr-}°R^4$
τ	Time	hr
φ	Angular location of NPU in orbit, latitude	radians
ω	Angle of incidence of suns rays on the earth	radians
Ω	Angular rate in orbit	radians

BLANK

APPENDIX II

A. MATHEMATICAL MODEL OF THE NPU DURING STARTUP

The basic equations used to describe the NPU during the startup phase of the flight are listed below. The heat transfer portions are based on the system nodal diagram (Figure 26).

1. Reactor Kinetics

The reactor kinetics equations are presented in normalized form.

a. Neutron Balance

$$\dot{N} = \frac{\beta}{\ell^*}\left(RN - N + \sum \frac{\beta_i}{\beta} C_i + R_o\right) \qquad \ldots(1)$$

where

$$\beta = \sum_{i=1}^{6} \beta_i$$

(1) Delayed Neutrons

$$C_i = \lambda_i(N - C_i); \quad i = 1, 2, 3, 4, 5, 6 \qquad \ldots(2)$$

(2) Total Reactivity

$$R = R_o + 2R_D + R_F + R_{GO} + R_{GI} \qquad \ldots(3)$$

$$R_D = f(\theta_D) \quad \text{(see Figure 24)} \qquad \ldots(4)$$

$$R_F = \int \frac{\partial R_F}{\partial T_F} d\bar{T}_F \qquad \ldots(5)$$

where

$$\frac{\partial R_F}{\partial \bar{T}_F} = f(\bar{T}_F)$$

$$R_{GO} = f(T_{GO}) \quad \ldots(6)$$

$$R_{GI} = f(T_{GI}) \quad \ldots(7)$$

b. Reactor Heat Transfer

(1) Fuel Heat Balance

$$M_{Fj} C_{PF} \dot{T}_{Fj} = K_j N + K_F \left[T_{F(j-1)} + T_{F(j+1)} - 2T_{Fj} \right] - \frac{UA}{3} (T_{Fj} - \bar{T}_{cj}) \quad \ldots(8)$$

$$j = 1, 2, 3$$

where

$$C_{PF} = f(\bar{T}_F)$$

$$UA = f(\bar{T}_R)$$

(2) Coolant Heat Balance

$$V_{cj} \rho_c C_{pc} \dot{T}_{cj} = \frac{UA}{3} (T_{Fj} - \bar{T}_{cj}) - \rho_c C_{pc} \dot{V} (T_{c(j-1)} - T_{cj}) \quad \ldots(9)$$

$$j = 1, 2, 3$$

where

$$\bar{T}_{cj} = \left[T_{c(j-1)} + T_{cj} \right] / 2$$

$$\rho_c C_{pc} = f(\bar{T}_R)$$

(3) Manifold Heat Balance

$$V_{MI} \rho_c C_{pc} \dot{T}_{MI} = K_{GI-MI} (T_{GI} - \bar{T}_{MI}) + \rho_c C_{pc} \dot{V} (T_{RI} - T_{MI}) \quad \ldots(10)$$

$$V_{MO} \rho_c C_{pc} \dot{T}_{MO} = K_{GO-MO} (T_{GO} - T_{MO}) + \rho_c C_{pc} \dot{V} (T_{c3} - T_{RO}) \quad \ldots(11)$$

(4) Grid Heat Balance

$$(MC_p)_{GI} \dot{T}_{GI} = K_{GI-MI} (\bar{T}_{MI} - T_{GI}) \quad \ldots(12)$$

$$(MC_p)_{GO} \dot{T}_{GO} = K_{GO-MO} (T_{MO} - T_{GO}) \quad \ldots(13)$$

c. Lines

Transport delay of the supply line

$$T_{UMi} = T_{PO}(t - \tau_{SL}) \qquad \ldots(14)$$

where

$$\tau_{SL} = \frac{V_{SL}}{\dot{V}}$$

Transport delay of the return line

$$T_{RI} = T_{LMo}(t - \tau_{RL}) \qquad \ldots(15)$$

where

$$\tau_{RL} = \frac{V_{RL}}{\dot{V}}$$

d. Converter – Radiator Heat Transfer

(1) Coolant Heat Balance

$$\sum (MC_p)_{cjk} \dot{T}_{cjk} = \rho_c C_{pc} \frac{\dot{V}}{2} (T_{c(j-1)k} - T_{cjk}) - K_{jk}(\overline{T}_{cjk} - T_{Mjk}) \qquad \ldots(16)$$

$$j = 1, 2, 3 \quad \text{and} \quad k = A, B$$

where

$$\overline{T}_{cjk} = \left[T_{c(j-1)k} + T_{cjk}\right]/2$$

(2) TE Material Heat Balance

$$\sum (MC_p)_{Mjk} \dot{T}_{Mjk} = K_{jk}(\overline{T}_{cjk} - T_{Mjk}) - G_{jk}(T_{Mjk} - T_{Rjk}) \qquad \ldots(17)$$

$$j = 1, 2, 3 \quad \text{and} \quad k = A, B$$

(3) Radiator Heat Balance

$$T_{RO} < T_{HS(eject.)} \quad \text{(with heat shield in place)}$$

$$\sum (MC_p)_{Rjk} \dot{T}_{Rjk} = G_{jk}(T_{Mjk} - T_{Rjk}) - \eta\sigma (A\epsilon F)_{Rjk}(T^4_{Rjk*} - T^4_{HSjk*}) \quad \ldots(18)$$

where * indicates absolute temperature.

$$T_{RO} > T_{HS(eject.)} \quad \text{(heat shield ejected)}$$

$$\sum (MC_p)_{Rjk} \dot{T}_{Rjk} = G_{jk}(T_{Mjk} - T_{Rjk}) - \eta\sigma\epsilon_R A_{Rjk}(T^4_{Rjk*} - T^4_{space*}) + Q_{s(Rjk)} \quad \ldots(19)$$

$$j = 1, 2, 3 \quad \text{and} \quad k = A, B$$

(4) Manifold Heat Balance

$$V_{MU}\rho_c C_{pc}\dot{T}_{MU} = \rho_c C_{pc}\dot{V}(T_{UMi} - T_{UM}) \quad \ldots(20)$$

$$V_{LM}\rho_c C_{pc}\dot{T}_{LMo} = \rho_c C_{pc}\dot{V}\left(\frac{T_{c3A} + T_{c3B}}{2} - T_{LMo}\right) \quad \ldots(21)$$

e. Heat Shield

$$(MC_p)_{HSjk}\dot{T}_{HSjk} = \eta\sigma\left[A\epsilon F\right]_{(R-HS)jk}\left(T^4_{Rjk*} - T^4_{HSjk*}\right) - \sigma(A\epsilon_o)_{HSjk}(T^4_{HSjk*} - T^4_{space*}) + Q_{s(HSjk)} \quad \ldots(22)$$

$$j = 1, 2, 3 \quad \text{and} \quad k = A, B$$

f. Solar Heating

Solar heating of side A of the NPU

$$Q_{sA} = Q_{TE} + Q_{DS} + Q_{RS} \quad \ldots(23)$$

Energy from thermal earth

$$Q_{TE} = \frac{F_{S\rightarrow E}\epsilon_E \sigma T_{E*}^4 (\epsilon A)_{jk}}{2} \quad \ldots(24)$$

(1) Direct Solar Energy

$$Q_{DS} = q_s(\alpha A_P)_{jk} f(\varphi) \quad \ldots(25)$$

(2) Reflected Solar Energy

$$Q_{RS} = \frac{q_s r_{E\rightarrow S} F_{S\rightarrow E} (\alpha A)_{jk} g(\varphi)}{2\varphi} \quad \ldots(26)$$

(3) Solar Heating of Side B of the NPU

$$Q_{sB} = Q_{sA}(2\pi - \varphi) \quad \ldots(27)$$

where

$$\varphi = \frac{2\pi}{P} t + \varphi_o$$

g. Control System

(1) Temperature-sensor switch heat balance

$$\dot{T}_{TS} = \frac{1}{\tau_{TS}} (T_{PO} - T_{TS}) \quad \ldots(28)$$

(2) Switch Status

$$S_s = f(T_{TS}) \quad \ldots(29)$$

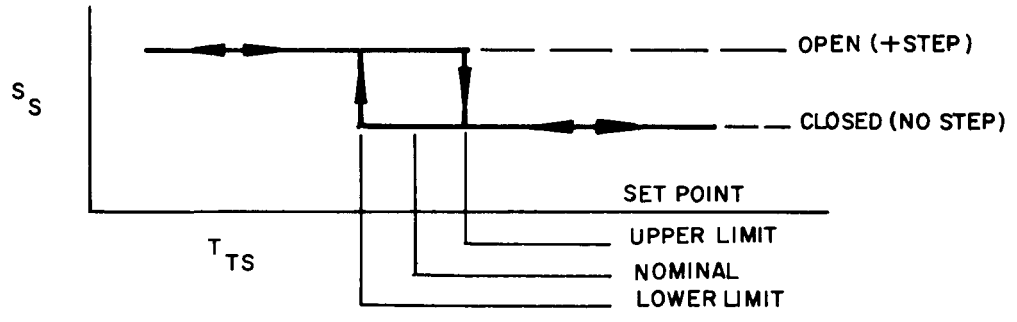

(3) Controller Status

for S_s changing from open to closed

$$C_s = f(S_s) \qquad \ldots(30)$$

for S_s changing from closed to open

$$C_s = f\left[S_s, (t - \tau_D)\right] \qquad \ldots(31)$$

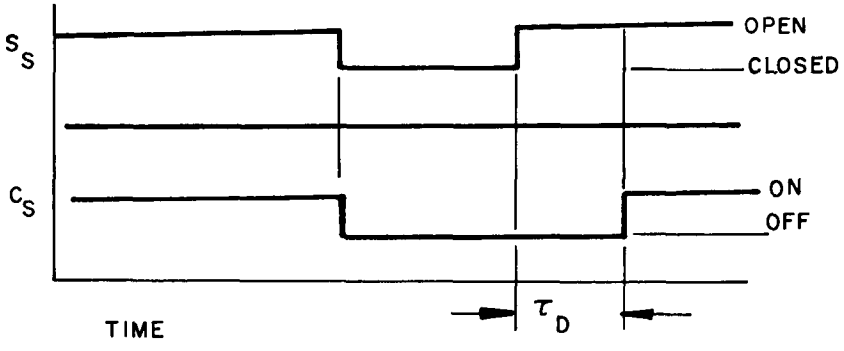

(4) Controller Output

$$E_o = O; \quad \text{for } C_s = OFF$$

$$E_o = \sum_{n=o}^{\infty} u_1(t + n\tau_{SR}); \quad C_s = ON \qquad \ldots(32)$$

(5) Drum Position

$$I_D\ddot{\theta}_D + b\dot{\theta} = kE_o \qquad \ldots(33)$$

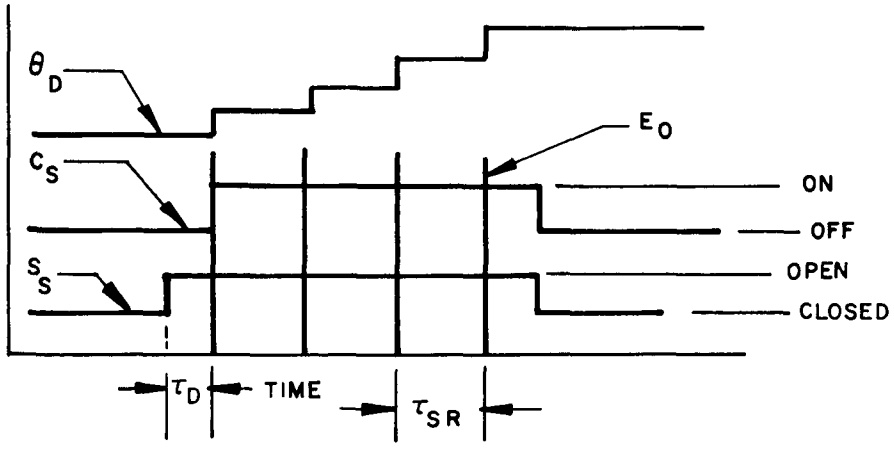

h. Pump Heat Transfer

(1) Coolant Heat Balance

$$V\rho_c C_{pc}\dot{T}_{PO} = \rho_c C_{pc}\dot{V}(T_{RO} - T_{PO}) - K_H(T_P - \overline{T}_H) \qquad \ldots(34)$$

where

$$T_P = (T_{RO} + T_{PO})/2$$

$$\overline{T}_H = (T_{HA} + T_{HB})/2$$

(2) Hot Junction Heat Balance

$$\sum (MC_p)\dot{T}_{Hk} = \frac{K_H}{2}(T_P - T_{Hk}) - K_{HC}(T_{Hk} - T_{Ck}) - \frac{I_{TE}\alpha_{PN}T_{Hk*}}{4} \qquad \ldots(35)$$

where

$$K_{HC} = f(\overline{T})$$

$$\alpha_{PN} = g(\overline{T})$$

(3) Cold Junction Heat Balance

$$\sum (MC_p)\dot{T}_{Ck} = K_{HC}(T_{Hk} - T_{Ck}) - K_{CR}(T_{Ck} - T_{Rk}) + \frac{I_{TE}\alpha_{PN}T_{Ck*}}{4} \qquad \ldots(36)$$

(4) Radiator Heat Balance

$$MC_p\dot{T}_{Rk} = K_{CR}(T_{Ck} - T_{Rk}) - \sigma\epsilon A_{Rk}(T^4_{Rk*} - T^4_{space*}) + Q_{s(Rk)} \qquad \ldots(37)$$

$$k = A, B$$

$$\overline{T} = (T_{HA} + T_{HB} + T_{CA} + T_{CB})/4 \qquad \ldots(38)$$

$$\Delta\overline{T}_P = \tfrac{1}{2}(T_{HA} + T_{HB}) - \tfrac{1}{2}(T_{CA} + T_{CB})$$

i. Pump and System Flow

(1) Force Balance at Pump Throat

$$I_{sys}\dot{w} = \frac{k_o B}{R'_p H'} E_w - \left[\frac{k_o k_B}{R'_p}\left(\frac{B}{H'}\right)^2 + \frac{k_{MH} B^2 \sigma_{NaK}}{H'}\right]\dot{V} - \Delta P_{FD} \quad \ldots(40)$$

where

$$\Delta P_{FD} = f(\dot{w})$$

$$\sigma_{NaK} = f(T_P)$$

(2) Voltage Summation

$$E_w = \alpha_{PN}\Delta\overline{T}_P - I_{TE}R'_{TE} \quad \ldots(41)$$

where

$$R'_{TE} = f(T)$$

(3) Current Summation

$$I_{TE} = \frac{\alpha_{PN}\left(\frac{1}{R'_B} + \frac{1}{R'_P}\right)\Delta\overline{T}_P - \frac{k_B B}{H'R'_P} V - I_s}{1 + \frac{R'_{TE}}{R'_B} + \frac{R'_{TE}}{R'_P}} \quad \ldots(42)$$

$$V = \frac{\dot{w}}{\rho_c} \quad \ldots(43)$$

B. NOMENCLATURE

Symbol	Description	Dimensions
N	Normalized neutron density	-
R	Reactivity	$
C	Normalized delayed neutron density	-
R_o	Reactivity with two coarse drums in	$
ℓ^*	Effective neutron mean lifetime	sec
t	Time	sec
$\dot{w}$	Coolant mass flowrate	lb/sec
T	Temperature	°F
C_p	Specific heat	kw-sec/lb-°F
M	Mass	lb
K, G	Thermal conductance	kw/°F
UA	Average fuel-coolant heat-transfer coefficient	kw/°F
$\dot{V}$	Coolant volumetric flowrate	$in.^3/sec$
V	Volume	$in.^3$
$\bar{T}_R$	Average reactor temperature	°F
T_{UMi}	Inlet temperature of converter upper manifold	°F
T_{LMo}	Outlet temperature of converter lower manifold	°F
$T_{HS(eject.)}$	Heat shield ejection temperature	°F
A	Area	$in.^2$
F	Geometrical or net interchange factor	-
Q_s	Solar heat input	kw
q_s	Solar constant	$kw/in.^2$
P	Orbit period	sec
r	Reflectivity	-
S_s	Temperature sensor switch status	-
C_s	Controller status	-
I_D	Actuator-drum inertia	$in.-lb-sec^2$
b	Actuator-drum constant	in.-lb-sec
kE_o	Driving torque	in.-lb
I_{TE}	Pump thermoelectric current	amp
I_{sys}	Inertia of coolant in the system	$sec^2/in.^2$
k_o	Proportionality constant	lb-in./amp-line

Symbol	Description	Dimensions
H'	Channel height of pump throat	in.
B	Magnetic flux across pump throat	lines/in.^{2}
k_B	Proportionality constant	-
k_{MH}	Magnetic-hydrodynamic imperical constant	-
E_w	Pump wall voltage	v
I_s	Pump external supply current	amp
R'_p	Resistance of coolant across the pump throat	ohm
R'_{TE}	Resistance of the pump TE stack	ohm
R'_B	Resistance of bypass paths around pump throat	ohm
Greek Letters		
β	Delayed neutron fraction	-
λ	Delayed neutron decay constant	sec^{-1}
ρ	Density	lb/in.^{3}
σ	Stefan-Boltzman constant	kw/in.^{2}-°R^4
ϵ	Thermal emissivity	-
η	Fin effectiveness	-
θ	Angular position of drums	deg
α	Solar absorptivity	-
φ	Angular position of NPU in orbit	deg
α_{PN}	Seebeck coefficient (N plus P material)	v/°F
σ_{NaK}	Coolant electrical conductivity	(ohm-in.)$^{-1}$
τ	Time constant	sec
τ_{SR}	Stepping period	sec
τ_D	Controller delay	sec
$\Delta\overline{T}_P$	Average temperature difference across pump TE material	°F
ΔP_{FD}	System pressure drop (including pump)	psi
Subscripts		
o	Initial	
GO	Upper gridplate	
GI	Lower gridplate	
F	Fuel	

Symbol	Description	Dimensions
c	Coolant	
RO	Reactor outlet	
RI	Reactor inlet	
MO	Upper reactor manifold	
MI	Lower reactor manifold	
D	Control drum	
*	Denotes absolute temperature	
i	Denotes i^{th} delay group	
j	Denotes j^{th} temperature node	
jk	Denotes j k^{th} temperature node	
SL	Supply line	
RL	Return line	
M	Converter TE material	
R	Radiator	
HS	Heat shield	
MU	Converter upper manifold	
LM	Converter lower manifold	
TE	Thermal earth	
DS	Direct sun	
RS	Reflected sun	
S	Sun	
E	Earth	
TS	Temperature sensor switch	
PO	Pump outlet temperature	
H	Hot junction	
C	Cold junction	
P	Pump throat	